

1 Reconciling single chamber Mg/Ca with whole shell $\delta^{18}\text{O}$ in surface to 2 deep dwelling planktonic foraminifera from the Mozambique Channel

3 Juliane Steinhardt¹, Caroline Cl  roux¹, Lennart de Nooijer¹, Geert-Jan Brummer^{1,2},
4 Rainer Zahn⁴, Gerald Ganssen², Gert-Jan Reichart^{1,3}

5
6 ¹ Department of Geology and Chemical Oceanography, NIOZ Royal Netherlands Institute for Sea Research, P.O. Box 59, NL-1790
7 AB Den Burg, Netherlands, * juliane.steinhardt@nioz.nl

8
9 ² Faculty of Earth- and Life Sciences, VU University Amsterdam, de Boelelaan 1085, 1081 HV Amsterdam, The Netherlands

10
11 ³ Department of Earth Sciences, Faculty of Geosciences, Utrecht University, P.O. Box 80021, 3508TA Utrecht, The Netherlands

12
13 ⁴ **Instituci   Catalana de Recerca i Estudis Avan  ats (ICREA) and Institut de Ci  ncia i Tecnologia Ambientals, Departament de F  sica,**
14 **Universitat Aut  noma de Barcelona, Cerdanyola del Vall  s, Spain.**

15
16 Corresponding author: juliane.steinhardt@nioz.nl

17 18 Abstract

19 Most planktonic foraminifera migrate vertically through the water column during life, meeting a
20 range of depth-related conditions as they grow and calcify. For reconstructing past ocean
21 conditions from geochemical signals recorded in their shells it is therefore necessary to know
22 vertical habitat preferences. Species with a shallow habitat and limited vertical migration will
23 reflect conditions of the surface mixed layer and short- and meso-scale (i.e. seasonal)
24 perturbations therein. Species spanning a wider range of depth habitats, however, will contain a
25 more heterogeneous, intra-specimen variability (e.g. Mg/Ca and $\delta^{18}\text{O}$), which is less for species
26 calcifying below the **thermocline**. Obtained single-chamber Mg/Ca are combined with single
27 specimen $\delta^{18}\text{O}$ and $\delta^{13}\text{C}$ of the surface water inhabitant *Globigerinoides ruber*, the thermocline-
28 dwelling *Neogloboquadrina dutertrei* and *Pulleniatina obliquiloculata* and the deep dweller
29 *Globorotalia scitula* from the Mozambique Channel. Species-specific Mg/Ca, $\delta^{13}\text{C}$ and $\delta^{18}\text{O}$ data
30 combined with a depth-resolved mass balance model confirm distinctive migration and
31 calcification patterns for each species as a function of hydrography. Whereas single specimen
32 $\delta^{18}\text{O}$ not always reveal changes in depth habitat related to hydrography (e.g. temperature),
33 measured Mg/Ca of the last chambers can only be explained by active migration in response to
34 changes in temperature stratification. Foraminiferal geochemistry and modeled depth habitats
35 shows that the single chamber Mg/Ca and single shell $\delta^{18}\text{O}$ are in agreement with each other
36 and in line with the changes in hydrography induced by eddies.

38 1. Introduction

39 Most planktonic foraminifera inhabit the upper 200 meters of the water column, with exceptions
40 of some species living as deep as 1000 m (e.g. Hemleben, 1989). The average depth habitat of
41 individual species and the range of water depths at which they are found reflect their ecology
42 (e.g. feeding behavior), ontogeny and seasonal preferences. Stable oxygen isotope values
43 ($\delta^{18}\text{O}$) and Mg/Ca ratios (Shackleton et al., 1974; Fairbanks et al., 1980; Ortiz et al., 1996;
44 Elderfield and Ganssen, 2000) have been used to reconstruct upper water column conditions
45 using species with a known depth range (e.g. Ravelo et al., 1992; Patrick and Thunell, 1997;
46 Faul et al., 2000; Cléroux et al., 2013). For many species, however, application of Mg/Ca as a
47 seawater temperature proxy is complicated by depth migration as a function of ontogeny.
48 Previous studies revealed major Mg/Ca heterogeneity within foraminiferal shells (e.g. Eggins et
49 al., 2003; Hathorne et al., 2009; Kunioka et al., 2006; Jonkers et al., 2012), which were
50 attributed to a combination of vertical migration during their life and vital effects. Nevertheless,
51 species-specific patterns of vertical migration and hence depth of calcification determine which
52 part of the water column can be reconstructed.

53 Field observations show that most foraminiferal species do not occupy a single depth, but rather
54 calcify at a range of depths. Many species migrate vertically as they grow and, therefore, the
55 chemical composition (e.g. Mg/Ca and $\delta^{18}\text{O}$) of their shells changes with age. Fairbanks et al.
56 (1982) and Field (2004) suggested that foraminifera may modify their habitat depth depending
57 on hydrographic condition and food supply. However, little is known about the exact controls on
58 depth habitat, termination of shell growth and controls on shell features (e.g. formation of crusts).
59 A better understanding of the vertical calcification pattern of different species is needed to
60 reconstruct past changes in vertical structure of the water column by using geochemical proxies,
61 e.g. for temperature ($\delta^{18}\text{O}$ and Mg/Ca). Using geochemical signals of species with different and
62 well-constrained calcification depths (Emiliani, 1954; Mulitza et al., 1997) changes in water
63 column conditions can be resolved.

64
65 Using core top samples from the Indian Ocean, Birch et al. (2013) report $\delta^{13}\text{C}$ and $\delta^{18}\text{O}$
66 measurements made on several species of planktonic foraminifera across a range of tightly
67 constrained size windows. From size controlled $\delta^{18}\text{O}$ calcite trajectories they inferred depth
68 habitats, using modern vertical temperature profiles. However, by using multiple core-top
69 specimens this data set encompasses not only vertical changes in the water column structure,
70 but also inter- and intra-annual changes therein, which are both known to vary substantially in
71 this region (e.g. McClanahan, 1988; Damassa et al., 2006; Hastenrath et al., 1993). In this study

72 we use sediment trap samples, allowing analyses of specimens that lived during a confined time
73 interval and link in situ hydrographic changes (i.e. temperature) more directly to their shell
74 chemistry.

75
76 Single-chamber Mg/Ca compositions from specimens with contrasting calcification depths (the
77 surface-dweller *Globigerinoides ruber* (d' Orbigny, 1839), the thermocline-dwelling species
78 *Neogloboquadrina dutertrei* (d' Orbigny, 1839) and *Pulleniatina obliquiloculata* (Parker et al.,
79 1865) and the deep dweller *Globorotalia scitula* (Brady, 1882) reflect temperatures throughout
80 the upper 500 m and were shown to reliably reflect short-term hydrographic changes (Steinhardt
81 et al., 2014). Meso-scale eddies such as observed in the Mozambique Channel (MC) induce
82 variations in temperature and salinity. Anticyclonic (anti-clockwise) eddies in the MC are
83 characterized by a warm water core and are associated with elevated sea surface heights and
84 large vertical isopycnal excursions. Foraminifera living in the mixed layer of the MC are affected
85 by eddy-induced changes, which is reflected by the geochemistry of *G. ruber* and *N. dutertrei*
86 (Steinhardt et al., 2014), resulting in higher Mg/Ca ratios and more depleted $\delta^{18}\text{O}_{\text{cc}}$ values.
87 These short-term changes in vertical water column temperature and $\delta^{18}\text{O}_{\text{sw}}$ distribution should
88 influence shell $\delta^{18}\text{O}$ and Mg/Ca throughout the different ontogenetic stages for any species
89 migrating during its life. Alternatively, foraminifera may respond to altered hydrographic
90 conditions by changing their calcification depth. Here we present combined single-specimen
91 $\delta^{18}\text{O}$ and single-chamber Mg/Ca measurements for different species, providing a composite of
92 thermocline and sub-thermocline conditions. Since single chamber Mg/Ca values cannot be
93 compared one-on-one with whole shell $\delta^{18}\text{O}$ -values we evaluate our results using a mass
94 balance model for depth related carbonate addition of four species of planktonic foraminifera.

95

96 **2. Oceanographic setting**

97 In the oligotrophic Mozambique Channel (MC) (Fig. 1) sea surface temperatures (SST) vary
98 seasonally and with eddy-induced transport (Fallet et al., 2011). The SSTs range from 25°C to
99 over 30°C with an annual mean of 27.6°C, the seasonal change in temperatures is associated
100 with the monsoon system. With the onset of Austral summer rainfall increases, caused by the
101 seasonal migration of the ITCZ and sea surface salinities decrease slightly from 35.2 in winter to
102 34.9 in summer (Fallet et al., 2010). Depth of the calcite compensation in the Western Indian
103 Ocean is below 3000 meters and hence promotes preservation of foraminiferal calcite at the
104 seafloor of the Mozambique Channel that has a depth of 2225 m at the trap location. Southward
105 migration of anticyclonic meso-scale eddies, originating at 10°S north off the Comoros Islands,

106 affects the hydrography in the MC (Fig. 1). Eddies pass through the MC at a mean frequency of
107 about four to seven per year (at a southward propagation speed of 3-6 km.d⁻¹) before joining the
108 Agulhas Current. An eddy passage is associated with vertical movement of isopycnals, which
109 can occasionally exceed 40 m per day in the upper layer (Ullgren et al., 2012). The formation of
110 meso-scale eddies in the Mozambique Channel is related to variability in the South Equatorial
111 Current (SEC) transport (Backeberg and Reason, 2010) (Fig. 1). The main water masses
112 contributing to the upper part of the MC include the Tropical Surface Water (TSW), Subtropical
113 Surface Water (STSW) and Indonesian Throughflow Water (ITFW). The warm, fresh surface
114 water (TSW) forms in the tropics and is transported westward within or north of the SEC (New et
115 al., 2007). In the proximity of the western margin, where the SEC bifurcates, warm surface
116 waters are transported poleward, either east of Madagascar, or through the MC (e.g. Gründlingh,
117 1995; Swallow et al., 1988). The STSW is characterized by relatively high salinities and a
118 subsurface maximum, with salinities of 35.2 – 35.5, at approximately 200 m below sea surface,
119 at which depth the surface water subducts below the fresher TSW (Wyrcki, 1973).

120

121 3. Material & Methods

122 3.1 Sediment trap and mooring array

123 Within the Long-term Ocean Climate Observations (LOCO) program, an array of eight moorings
124 across the narrowest part of the Mozambique Channel, provides continuous measurements of
125 current velocities, temperatures and salinities at fixed depths since November 2003 (Ullgren et
126 al., 2012). Sediment traps of the type Technicap PPS 5 were deployed at 16.8°S and 40.8°E in
127 the central MC (Fig. 1), equipped with an automated sampling carousel of 24 cups and a baffled
128 collecting area of 1 m². The trap was positioned 250 m above the channel floor at 2250 m water
129 depth. Between November 2003 and February 2009, a total of four sediment trap deployments
130 took place, each programmed to a 17, 21 or 23 days sampling interval. Prior to deployments,
131 sample cups were filled with an HgCl₂-poisoned and borax-buffered solution of seawater
132 collected from the deployments depth (Lončarić et al., 2007). Sediment trap samples were wet-
133 split, sieved and foraminiferal shells were cleaned according to the protocol of Barker et al.
134 (2003), modified after Fallet et al. (2009) (Fallet et al., 2010; Steinhardt et al., 2014).

135 Using sediment trap material allows to link the chemistry of the shells to actual ambient *in situ*
136 measurements from the moorings and from real-time satellite derived observations. Therefore
137 we are able to link short time changes in hydrography (i.e. eddies) to the differences in shell
138 chemistry. Calculated back trajectories, based on a high-resolution INALT01 model (Durgadoo,
139 2013), show that specimens ending up in the sediment trap all originate from the area under

140 influence of the eddy-variability (Steinhardt et al., 2014). We selected the sediment trap intervals
141 during which the complete sediment cup collection took place under either full eddy or full non-
142 eddy conditions (for full description see Steinhardt et al., 2014; supplement). For the selected
143 collecting intervals, temperature and salinity observations from the mooring (lmc5a) are
144 compiled and daily means were used to calculate eddy and non-eddy temperature profiles.

146 3.2 Temperature and Salinity data

147 For this study, we used temperatures recorded at 110 m; 200 m and 400 m water depth by a
148 CTD deployed on mooring lmc5A (16.8°S, 41.1°E, Fig. 1), which is closest to the sediment trap
149 site. Moored salinity and temperature data, collected during the selected intervals of eddy and
150 non-eddy conditions (Table S1 in the Supplement), was spline fitted in Analyseries 1.1.6 68K to
151 achieve meter-wise data resolution. Sea surface temperatures were retrieved from the 4 km
152 daytime MODIS/AQUA dataset around trap site (16 – 17°S and 40 – 41°E) for the period of the
153 selected collecting intervals (<http://poet.jpl.nasa.gov/>). Surface salinity data is not available for
154 the complete deployment period and instead, CTD-based salinity-depth profiles taken during the
155 deployment/recovery cruises were used (Ullgren et al., 2012). Based on the trend observed in
156 the moored salinity data at 110 m water depth (Ullgren et al., 2012; less saline during eddy
157 condition) we use CTD minimum surface salinities to represent eddy surface salinities and
158 maximum surface salinities to represent non-eddy conditions. Since salinity mooring data was
159 non-existent between 400 and 1525 m, we have chosen two more "anchor points" at 700 and
160 1000 m water depth from the CTD depth profiles in order to better capture the Red Sea Water
161 (RSW) advection at these depths and to achieve a more accurate salinity fitting curve for the
162 upper 1000 m.

164 3.3 Planktonic foraminiferal species and ontogeny

165 We selected four species from the sediment trap samples according to differences in depth
166 habitats as reported in previous studies. *Globigerinoides ruber* (white) is a shallow, surface
167 mixed layer dwelling species, occupying the upper 50 m of the water column and is commonly
168 used to reconstruct paleo-SST (Hemleben et al., 1989). To minimize a potential biases in $\delta^{18}\text{O}$
169 and Mg/Ca associated when combining different morphotypes (Steinke et al., 2005), we used
170 only *G. ruber* sensu stricto that was by far the most abundant in these samples (Fallet et al.,
171 2010).

172 The subsurface-dwellers *Neogloboquadrina dutertrei* and *Pulleniatina obliquiloculata* have been
173 associated with a calcification depth of 0 - 100 meters and 60 - 150 meters in the upper and

174 middle thermocline, respectively (Erez and Honjo, 1981; Fairbanks et al., 1982; Ravelo and
175 Fairbanks, 1992; Spero et al., 2003; Field, 2004; Kuroyanagi and Kawahata, 2004; Huang et al.,
176 2008). The deep-dwelling species *Globorotalia scitula* was used as a representative for deep
177 water conditions (Bé, 1969; Ortiz et al., 1996; Itou et al., 2001; Fallet et al., 2011).
178 Measurements on *G. ruber* were usually performed on specimens in the 250 - 315 μm size
179 fraction. In a limited number of samples, abundances of this species were low in this size
180 fraction, and geochemical analyses were therefore performed on specimens from a larger size
181 fraction (315 - 400 μm). Analyses on *N. dutertrei*, *P. obliquiloculata* and *G. scitula* were generally
182 done on the size range $>315 \mu\text{m}$, with additional measurements on the 250 - 315 μm size
183 fraction depending on the specimen's abundance within a sample. All specimens show excellent
184 preservation and do not show any signs of diagenesis (based on SEM microscopy). Recently,
185 Fallet et al. (2012) showed that shell size normalized weights of three species of planktonic
186 foraminifera from the same sediment trap location do not differ from those of the surface
187 sediment samples below this trap. Absence of dissolution is also reported by Birch et al. (2013)
188 describing planktonic foraminifera from surface sediments at $\sim 3000 \text{ m}$ water depth, in the
189 northern part of the Mozambique Channel, as being glassy and preserved excellently.

190

191 3.4 Mg/Ca and Stable isotope analyses

192 The Mg/Ca ratios of single chambers used in this study were previously published (Steinhardt et
193 al., 2014) and were determined by Laser Ablation-Inductively Coupled Plasma-Mass
194 Spectrometry (LA-ICP-MS) at Utrecht University (Reichert et al., 2003) (for summary of the
195 results see Tab. 1). Subsequently, specimens were analyzed for whole shell $\delta^{18}\text{O}$ and $\delta^{13}\text{C}$ after
196 microscopic removal from the laser ablation stub with ethanol and inspection for possible
197 contaminations. Measurements were performed at the Universitat Autònoma de Barcelona on a
198 Thermo Finnigan MAT253 mass spectrometer coupled to a Kiel IV device for CO_2 sample gas
199 preparation. External reproducibility (1σ) of $\delta^{13}\text{C}$ standards NBS19 and IAEA-CO was 0.04‰
200 and for $\delta^{18}\text{O}$ 0.08‰.

201 Single shells from part of the sample set were analyzed using a Thermo Finnigan Delta Plus
202 mass spectrometer equipped with a Gas Bench II preparation device at the VU University
203 Amsterdam. Single specimens were loaded into round-bottom vials, which were subsequently
204 flushed with He. The samples then reacted with phosphoric acid (H_3PO_4) injected into the vial
205 producing CO_2 gas, which is transported in a helium stream to the mass spectrometer. Traps are
206 used to remove residual H_2O from the sample gas and the CO_2 is separated from other possible
207 contaminant gases on a poraplot Q GC column. Reproducibility (1σ) of $\delta^{13}\text{C}$ standards NBS19

208 and was 0.07‰ and for $\delta^{18}\text{O}$ 0.12‰. Values measured on the Kiel IV and the GASBENCH-II are
209 comparable and species-specific $\delta^{18}\text{O}_{\text{CC}}$ are in good agreement (Tab. 2). Measurements with the
210 GASBENCH-II have a somewhat wider standard deviation inherent to continuous flow mass
211 spectrometry. In total, 391 single shell stable isotope values were obtained. Values deviating
212 more than twice the standard deviation from the average of the total dataset were regarded as
213 outliers (n=23) and removed from the dataset.

214 The $\delta^{18}\text{O}_{\text{sw}}$, expressed on the SMOW scale is converted to Pee Dee Belemnite (PDB) scale by
215 subtracting 0.27‰ (Hut, 1987). Various $\delta^{18}\text{O}$ -temperature equations have been proposed and
216 discussed in detail in other studies (Bemis et al., 1998; Regenberg et al., 2009), without clear
217 consensus on the most appropriate equation. Here, we integrated calcification depth for each
218 species calculated by matching the foraminiferal calcite $\delta^{18}\text{O}_{\text{CC}}$ with the calculated calcite $\delta^{18}\text{O}_{\text{calc}}$
219 following equation (1) from Kim and O'Neil (1997) for the temperature dependent fractionation of
220 calcite by inorganic precipitation (assuming calcification in equilibrium with the ambient
221 seawater).

222

$$223 \quad (1) \delta^{18}\text{O}_{\text{eq}} = 25.778 - 3.333 \times \sqrt{43.704 + T} + (\delta^{18}\text{O}_{\text{sw}} - 0.27)$$

224

225 We extracted $\delta^{18}\text{O}_{\text{sw}}$ values from the South Indian Ocean for the upper 2000 m (4.5 - 120.2°E; 0
226 - 32.9°S, N=154) from the Global Seawater Oxygen-18 Database (see supplementary table,
227 <http://data.giss.nasa.gov/o18data/>). Additionally we included in situ $\delta^{18}\text{O}_{\text{sw}}$ measurements from
228 the MC, near the sediment trap location (41.08°E; 16.74°S) in order to determine the regional
229 relationship between $\delta^{18}\text{O}_{\text{sw}}$ and salinity (Eq. 2)

$$230 \quad (2) S = 0.463 * \delta^{18}\text{O}_{\text{sw}} - 15.9, r^2 = 0.87$$

231 This linear relationship (3) is subsequently used to estimate $\delta^{18}\text{O}_{\text{sw}}$ values based on salinities
232 measured in the proximity of the trap by moored T-S sensors during eddy and non-eddy
233 conditions for depths ranging from 0 to 1000 m.

234 Seawater temperature and estimated $\delta^{18}\text{O}_{\text{sw}}$ profiles for eddy or non-eddy conditions are used to
235 compare the $\delta^{18}\text{O}$ data depending on the time interval sampled by the sediment trap. We used
236 averaged $\delta^{18}\text{O}_{\text{sw}}$ from the depth range suggested by previously measured single chamber
237 Mg/Ca analyses (Steinhardt et al., 2014), to calculate the $\delta^{18}\text{O}$ -derived calcification temperature
238 for all species, following the temperature equation of Kim and O'Neil (1997):

239

$$240 \quad (3) T = 16.1 - 4.64 * (\delta^{18}\text{O}_{\text{CC}} - (\delta^{18}\text{O}_{\text{sw}} - 0.27)) + 0.09 * (\delta^{18}\text{O}_{\text{CC}} - (\delta^{18}\text{O}_{\text{sw}} - 0.27))^2$$

241 The temperature equation of Kim and O'Neil (1997) is the most general calibration, which allows
242 comparing inter specific differences that are automatically accounted for when using species-
243 specific calibrations.

244

245 4. Results

246 4.1 Oxygen isotopes

247 Single specimen values of $\delta^{18}\text{O}_{\text{CC}}$ range from -3.50‰ to 2.65‰. Although the values measured
248 on individual specimens clearly overlap, each species has a different average $\delta^{18}\text{O}_{\text{CC}}$ and $\delta^{13}\text{C}_{\text{CC}}$
249 (Fig. 2 and 3). The $\delta^{18}\text{O}_{\text{CC}}$ values are most depleted for *G. ruber*, somewhat more enriched in
250 comparison to *G. ruber* for *P. obliquiloculata* and *N. dutertrei*, with most enriched values in *G.*
251 *scitula* (Tab. 1, Fig. 2 and 3). The relationship between temperature and $\delta^{18}\text{O}_{\text{CC}}$ is generally
252 described with more depleted $\delta^{18}\text{O}_{\text{CC}}$ values indicating higher temperatures and thereby
253 shallower calcification depths. Thus, each species has a distinct whole shell- $\delta^{18}\text{O}$ signature,
254 reflecting their different mean calcification depth. *G. ruber* ($-2.57 \pm 0.04\text{‰}$, SD: $\pm 0.24\text{‰}$), *N.*
255 *dutertrei* and *P. obliquiloculata* record negative $\delta^{18}\text{O}_{\text{CC}}$ values between $-1.53 \pm 0.03\text{‰}$ (standard
256 deviation (SD): $\pm 0.42\text{‰}$) and $-1.13 \pm 0.04\text{‰}$ (SD: $\pm 0.24\text{‰}$), more noticeable positive values are
257 found for *G. scitula* with $1.47 \pm 0.14\text{‰}$ (SD: $\pm 0.87\text{‰}$) (Fig. 3). No significant trend between size
258 fractions and stable isotopes was observed for any of the analyzed species over the size range
259 we used, as confirmed by ANOVA tests (Kruskal-Wallis one way analysis of variance on ranks)
260 of $\delta^{18}\text{O}_{\text{CC}}$ between the size fractions (*G. ruber*: $p=0.774$, *N. dutertrei*: $p=0.500$, *G. scitula*: $p=$
261 0.373).

262 No significant differences in $\delta^{18}\text{O}$ values for *G. ruber* and *N. dutertrei* were found between eddy
263 and non-eddy conditions. In the deeper dwelling species *P. obliquiloculata* ($U=54$, $P=0.04$) and
264 *G. scitula* ($U=80$, $P=0.021$), most depleted $\delta^{18}\text{O}$ values were found during eddy conditions and
265 non-eddy conditions, respectively (Tab. 3; Fig. 3).

266

267 4.2 Carbon isotopes

268 Values for $\delta^{13}\text{C}$ range from -1.5‰ to 2.0‰. Most enriched $\delta^{13}\text{C}$ values are found in *N. dutertrei*
269 ($\delta^{13}\text{C}=0.53 \pm 0.042\text{‰}$, SD: $\pm 0.44\text{‰}$), whereas values for *P. obliquiloculata* are most depleted
270 ($\delta^{13}\text{C}=0.04 \pm 0.04\text{‰}$, SD: $\pm 0.21\text{‰}$). Individuals of *G. ruber* reflect a relatively large range in $\delta^{13}\text{C}_{\text{CC}}$
271 values ($0.51 \pm 0.04\text{‰}$, SD: $\pm 0.47\text{‰}$), whereas *G. scitula* ($0.27 \pm 0.04\text{‰}$, SD: $\pm 0.22\text{‰}$) displays a
272 much more limited variability in $\delta^{13}\text{C}_{\text{CC}}$ (Tab. 1, Fig. 3). Species specific $\delta^{13}\text{C}$ - $\delta^{18}\text{O}$ relationships
273 (Fig. 2) differ and only *G. scitula* showed a positive correlation between single specimen carbon
274 and oxygen isotope ratios (Fig. 2, $r^2=0.388$, $p<0.001$). Moreover, values for *G. scitula* differ from

275 those of other species, with relatively depleted $\delta^{13}\text{C}$ (0.27‰, SD: $\pm 0.22\%$) and relatively
276 enriched $\delta^{18}\text{O}$ values (1.47‰, SD: $\pm 0.87\%$).

277 From the four investigated species, only *G. scitula* (N: 37) did not show a significant difference in
278 $\delta^{13}\text{C}$ between eddy and non-eddy conditions. *G. ruber* (N: 200; Mann-Whitney rank sum test U=
279 3373, $p = 0.002$), and *P. obliquiloculata* (N: 33; U= 52, $p = 0.032$) showed significantly more
280 positive $\delta^{13}\text{C}$ values during non-eddy conditions. During non-eddy condition however, *N.*
281 *dutertrei* (N: 118; U= 939.5, $p = 0.002$) recorded more negative $\delta^{13}\text{C}$ values (Fig. 3).

282

283 4.3 Calcification temperatures

284 The calculated multi-specimen $\delta^{18}\text{O}$ -based temperature from eq. (3) and the single chamber
285 Mg/Ca are positively, exponentially correlated (Fig. 4). Variability in this relationship is highest at
286 higher ($> 25^\circ\text{C}$) temperatures. Mg/Ca-derived calcification temperatures, for *G. ruber* are on
287 average $28.1 \pm 2.8^\circ\text{C}$, based on the calibration of Fallet et al. (2010) for this species in this region.
288 Calcification temperatures for *N. dutertrei* and *P. obliquiloculata* are $22.5 \pm 3.7^\circ\text{C}$ and $21.6 \pm 3.1^\circ\text{C}$,
289 respectively, both based on species-specific calibrations from Anand et al. (2003). Mg/Ca ratios
290 of *G. scitula* were transformed into temperatures using the equation for *G. hirsuta* (Anand et al.,
291 2003) resulting in an average temperature of $14.4 \pm 3.4^\circ\text{C}$ (Fig. 5). Calcification temperatures
292 based on $\delta^{18}\text{O}$ result in markedly different values, ranging from $29.4 \pm 1.3^\circ\text{C}$ for *G. ruber* to
293 $24.4 \pm 2^\circ\text{C}$ for *N. dutertrei*, $22.5 \pm 1.1^\circ\text{C}$, for *P. obliquiloculata* and $10.4 \pm 3.9^\circ\text{C}$ for *G. scitula* (Tab.
294 1). Since *P. obliquiloculata* and *G. scitula* showed significant differences for $\delta^{18}\text{O}_{\text{CC}}$ between
295 eddy and non-eddy conditions, we separately calculated temperatures for eddy and non-eddy
296 condition. Mean $\delta^{18}\text{O}$ from Eq. (3) for eddy intervals yield $22.8 \pm 0.9^\circ\text{C}$ for *P. obliquiloculata* and
297 $7.9 \pm 2.1^\circ\text{C}$ for *G. scitula*. For non-eddy intervals calcification temperatures are $22.5 \pm 1.2^\circ\text{C}$ for *P.*
298 *obliquiloculata* and $11.8 \pm 4.1^\circ\text{C}$ for *G. scitula* (Fig. 5).

299

300 5. Discussion:

301 5.1 Single specimen isotope temperatures

302 The average, single-specimen $\delta^{18}\text{O}_{\text{CC}}$ of *G. ruber* reflect SSTs of $27.0 \pm 2.2^\circ\text{C}$ - $28.4 \pm 2.1^\circ\text{C}$
303 (based on sediment-trap calibrations from Fallet et al., 2010 and Wilke et al., 2009, respectively),
304 which is close to the satellite-derived annual mean SST of 27.6°C (Fallet et al., 2010). When
305 applying the equation of Kim and O'Neil (1997) for conversion of $\delta^{18}\text{O}_{\text{CC}}$ into temperature SST is
306 considerably higher ($29.4 \pm 1.3^\circ\text{C}$). This discrepancy, may be caused by the fact that the calcite-
307 water calibration of Kim and O'Neil (1997) is based on inorganic precipitation experiments, free

308 of vital effects and therefore may be offset compared to the temperature- $\delta^{18}\text{O}_{\text{CC}}$ relationship of
309 biogenic carbonates. Nevertheless this temperature estimate based on Kim and O'Neil (1997) is
310 in good agreement with the average temperature of $28\pm 1.1^\circ\text{C}$ during the investigated intervals.
311 The intertest variability of this species can be explained by the high temperature variability at the
312 sea surface, as well as differences in symbiont activity. The shallow depth habitat of *G. ruber* in
313 the MC is in line with previous studies showing that this species is confined to the photic zone
314 (e.g. Deuser et al., 1981; Lončarić et al., 2006; Peeters and Brummer, 2002), because of the
315 light requirement of its symbionts. Based on its relatively narrow preferred depth habitat, this
316 species is a suitable tracer for (sub)tropical surface-water (0 - 100 meters, mixed layer)
317 conditions (e.g. Deuser, 1987; Anand et al., 2003; Field, 2004; Fallet et al., 2010). Birch et al.
318 (2013) show that shell size of specimens of *G. ruber* is not correlated to $\delta^{18}\text{O}_{\text{CC}}$, confirming that
319 this species occupies a narrow calcification depth during its life. In addition to its shallow living
320 depth, *G. ruber* is known to occur in some areas relatively equally throughout the year (e.g.
321 Deuser, 1987; Mohtadi et al., 2006; Tedesco et al., 2007), whereas in other areas, including the
322 MC, they occur at highest densities during summer months (e.g. Tolderlund and Bé, 1971;
323 Duplessy et al., 1981; Ganssen and Sarthein, 1983; Deuser and Ross, 1989; Eguchi et al.,
324 2003; Lončarić et al., 2006; Fallet et al., 2010). This seasonal preference results in SSTs that
325 are slightly biased towards summer conditions when using fossil specimens of this species.

326
327 Based on an average $\delta^{18}\text{O}_{\text{CC}}$ -derived temperature of $24.3\pm 2^\circ\text{C}$ (Tab. 2), following the equation of
328 Kim and O'Neil (1997), calcification depths of *N. dutertrei* are in the range of 20 - 130 m (Fig. 6)
329 with an average of 58 m. For eddy conditions, the average calcification depth is approximately
330 80 m, for non-eddy condition it is approximately 37 m. Average Mg/Ca-based temperature of
331 $22.5\pm 4^\circ\text{C}$ is in relatively good agreement with the average $\delta^{18}\text{O}_{\text{CC}}$ -derived temperature (Tab. 2).
332 The difference between Mg/Ca- and $\delta^{18}\text{O}$ -based temperatures are smaller than the 1.2°C
333 uncertainty associate with the Mg/Ca calibration (Anand et al., 2003). Previous studies using *N.*
334 *dutertrei* from Indian Ocean core top samples and Mozambique Channel sediment traps have
335 reported similar depth ranges between 40 - 150 m (Kiefer et al., 2006) and similar average
336 depths of 80 m (Fallet et al., 2011), respectively. Both of these studies used pooled specimen for
337 their stable isotope analysis and hence provided the population's average calcification depth.
338 Moreover, pooling of specimens from sediment core samples (Kiefer et al., 2006) does not allow
339 for resolving short-term variability in calcification temperatures as do single specimens (e.g.
340 seasonality). The inferred calcification depth for *N. dutertrei* is in line with its characterization as
341 an intermediate deep dwelling species, living preferentially in the seasonal thermocline (e.g.

342 Fairbanks et al., 1982; Curry et al., 1983; Eguchi et al., 2003; Farmer et al., 2007), coinciding
343 with a deep chlorophyll maximum (Fairbanks et al., 1980; Ravelo et al., 1990). Overall living
344 depth of this species is confined to the upper 200 m (Farmer et al., 2007; Kroon and Darling,
345 1995). Variability in Mg/Ca within single specimen shell walls of *N. dutertrei* from the Timor Sea
346 suggested temperatures between 12 and 23°C, implying migration through the entire
347 thermocline (Eggins et al., 2003). However, most calcification seems limited to a much smaller
348 depth interval and the extremes in Mg/Ca might reflect upper and lower depth limits occupied by
349 this species. Moreover, banding of Mg/Ca in shell calcite has been viewed in terms of discrete
350 calcification events (Elderfield et al., 1996; Erez et al., 2003). Plankton tow studies (Fairbanks et
351 al., 1980) showed oxygen isotope equilibrium calcification for *N. dutertrei* and *P. obliquiloculata*.

352
353 The $\delta^{18}\text{O}_{\text{CC}}$ -based calcification depths for *P. obliquiloculata* reported here (48-125 m, with an
354 average of 74 m, Fig. 6) are in close agreement with those reported previously (e.g. between 60
355 and 80 m; Mohtadi et al., 2009). Indeed, in plankton tows from the central equatorial Pacific the
356 largest abundance of adult *P. obliquiloculata* with a terminal cortex was found below 60 m
357 (Watkins et al., 1996). All specimens used in this study had the distinctive smooth outer cortex
358 that envelops the final whorl in the adult as well as an arched aperture (Watkins et al., 1996).
359 Non-corticated *P. obliquiloculata* (“juveniles”) are confined mostly to the mixed layer (Watkins et
360 al., 1996), indicating migration to greater depths at the time of cortex formation during the
361 terminal stage of its life cycle (Erez and Honjo, 1981; Hemleben et al., 1989; Ravelo and
362 Fairbanks, 1992).

363 The average $\delta^{18}\text{O}_{\text{CC}}$ for *G. scitula* yields a calcification temperature of $10.4 \pm 3.9^\circ\text{C}$, suggesting
364 that this species calcifies between 175 and 1100 m (Fig. 6) with an average of approximately
365 500 m. However, previous studies indicated that $\delta^{18}\text{O}$ -derived temperatures of *G. scitula* are
366 associated with a vital effect of -1.16‰ positively off-setting temperatures by approximately 4°C
367 (e.g. Kahn and Williams, 1981; Fallet et al., 2011; Birch et al. 2013). Subtracting the suggested
368 vital effect, the actual ambient seawater temperature at the inhabited depth would be
369 $14.4 \pm 3.9^\circ\text{C}$, which elevates the inferred average calcification depth to 300 m (ranging between
370 175 and 500 m). The vital effect corrected temperature compares very well with the Mg/Ca-
371 based temperature of $14.4 \pm 3.4^\circ\text{C}$.

372 Birch et al. (2013) support previous findings of a distinct positive correlation between $\delta^{18}\text{O}$ and
373 size in *G. scitula* (e.g. Friedrich et al., 2012), which is linked to a substantial ontogenetic vertical
374 migration through the water column. Largest individuals have been inferred to live below the
375 thermocline, consistent with the supposed absence of symbionts in this species. This is in line

376 with our observations, showing higher inter-specimen variability in $\delta^{18}\text{O}_{\text{cc}}$ for *G. scitula*, than in
377 the other species.

378

379 **5.2 Habitat depth versus calcification depth**

380 Planktonic foraminifera collected by sediment traps might record $\delta^{18}\text{O}_{\text{cc}}$ signals comprising
381 calcification at various depths and thus document an *apparent* average calcification depth by
382 integrating the entire calcification history of the specimen. Given changes in seawater
383 temperature with water depth, even minor changes in the upper or lower range of the depth at
384 which planktonic species calcify, can have a profound effect on the average $\delta^{18}\text{O}_{\text{cc}}$ and
385 reconstructed temperature. Since evidence is accumulating that some species have a flexible
386 calcification range (e.g. due to seasonality or local hydrography; Lončarić et al., 2006; Wilke et
387 al., 2009), interpretation of down core stable isotope data in terms of thermal structure may be
388 challenging. Therefore, it is crucial to accurately quantify the impact of environmental factors on
389 depth preferences of planktonic foraminifera. Contrasting eddy and non-eddy conditions, a
390 short-term feature, allow us to disentangle seasonal and other short-term local hydrography
391 changes and their effect on foraminiferal calcification depth.

392 While Mg/Ca-based temperatures of *G. ruber* and *N. dutertrei* record eddy induced changes in
393 upper water column stratification (Steinhardt et al., 2014), $\delta^{18}\text{O}$ -based temperatures are
394 relatively similar for both species (Fig. 6). Using the paleo-temperature equation (equation (1);
395 Kim and O'Neil, 1997) and fitting $\delta^{18}\text{O}_{\text{calc}}$ with $\delta^{18}\text{O}_{\text{cc}}$, we find that *G. ruber* calcifies on average at
396 the sea surface (down to 7 m during non-eddy conditions and down to 18 m under eddy
397 conditions) (Fig. 6). *N. dutertrei* calcifies on average between 12 and 120 m during eddy
398 conditions (average calcification depth 81 m) and between 17 and 58 m under non-eddy
399 conditions (average 37 m). During eddy conditions, *P. obliquiloculata* calcifies between 89 and
400 124 m (average 107 m), whereas it calcifies at shallower depth, between 20 and 77 m (average
401 calcification depth 60 m) during non-eddy condition. Largest changes in calcification depth in this
402 study are inferred from *G. scitula*. From a calcification range between 503 to 1098 m and an
403 average calcification around 716 m during eddy condition it shifts to a calcification range from
404 168 to 745 m and an average calcification depth of 343 m (Fig. 6). If we apply the suggested
405 4°C offset for *G. scitula* calcification depth ranges shoal during eddy condition to 303 to 515 m
406 (average 387 m) and during non-eddy to 95 to 350 m (average 178 m).

407

408 Conversely, $\delta^{18}\text{O}$ -based temperatures are significantly different for *P. obliquiloculata* and *G.*
409 *scitula*, while the Mg/Ca-based temperature of the last formed chambers of *P. obliquiloculata*

410 indicate similar calcification temperature (Tab. 1). Mg/Ca inferred calcification temperatures,
411 representing the depth occupied at the later stages of the foraminifer's life, were similar between
412 eddy and non-eddy conditions. Nonetheless, temperature mooring data show a steep
413 temperature gradient, coinciding with the habitat depth of *G. scitula*, and thereby revealing a
414 wide range of calcification depths for this species, changing significantly with deepening of the
415 thermocline during eddy passage.

416
417 Inferred higher variability in calcification temperature for *G. ruber* presented in this study
418 compared to observed satellite SST likely results from the spatial resolution employed here.
419 Inter-individual differences in depth migration add to the variability in isotopes and element/Ca
420 ratios when measuring single specimens. Potential effects of ontogeny on stable isotope
421 composition are minimized by using narrow size fractions, as confirmed by the lack of
422 ontogenetic trends with shell size in our measurements. Russell and Spero (2000) concluded
423 that natural variability in oxygen isotopes is species specific. Measuring single specimen $\delta^{18}\text{O}_{\text{cc}}$
424 of *G. ruber* shells from sediment traps in the eastern equatorial Pacific, they show that over a 1.5
425 – 3 day period, the standard deviation of $\delta^{18}\text{O}$ results in a temperature variability of $\pm 0.87^\circ\text{C}$.
426 Such a variability could explain between 12 and 38% of the variability in $\delta^{18}\text{O}$ -based
427 temperatures in our samples. Another cause of natural variability might be differences in depth
428 at which an individual calcifies. In laboratory cultures, the addition rate of new chambers in *G.*
429 *sacculifer* ranges from 1.6 to 6.2 days (Bé, 1981), while chamber formation in *G. hirsuta* and *G.*
430 *truncatulinoidea* takes about 5 to 6 hours (Bé, 1979). Considering that our sample duration
431 ranges between 17 and 21 days, $\delta^{18}\text{O}$ variability is likely to be affected by other parameters (e.g.
432 temperature). Therefore, the observed variability in $\delta^{18}\text{O}$ -based temperatures caused by species
433 specific natural variability in $\delta^{18}\text{O}_{\text{cc}}$ (e.g. Russell and Spero, 2000) during the time it takes to add
434 new chambers, which might be calcified under different conditions or water depth.

435 436 **5.3 Reconciling $\delta^{18}\text{O}$ and Mg/Ca-derived calcification depths**

437 Mg/Ca-derived temperatures indicate that calcification depths of *N. dutertrei* range between 42-
438 169 m (average depth: 81 m) under non-eddy conditions and between 13 and 196 m (average
439 depth: 98 m) during eddy conditions (Steinhardt et al., 2014). Thus, the shoaling in average
440 calcification depth from 98 m during eddy conditions to 81 m during non-eddy conditions,
441 indicated by the whole shell $\delta^{18}\text{O}_{\text{cc}}$ is less as than inferred from Mg/Ca, derived from the
442 calcification of the last chambers. A more pronounced trend is present in Mg/Ca of *P.*
443 *obliquiloculata*, shifting between 70 and 90 m (average 75 m) during non-eddy conditions, to

444 depths between 147 and 244 m (average 150 m) during eddy conditions (Steinhardt et al.,
445 2014). The Mg/Ca-derived shift is hence larger than the shift inferred from $\delta^{18}\text{O}_{\text{CC}}$ (eddy: 107 m
446 and non-eddy: 60 m). Mg/Ca-derived calcification temperatures for *N. dutertrei* and *P.*
447 *obliquiloculata* are hence cooler and indicative of deeper calcification of the final chambers
448 compared to that of the whole shell (based on $\delta^{18}\text{O}_{\text{CC}}$). Calcification temperatures derived from
449 Mg/Ca for *G. scitula* (Fig. 5), indicate an opposite trend, shifting between 257 and 320 m
450 (average 340 m) during eddy conditions to shallower depths between 265 and 287 m (average
451 230 m) during non-eddy conditions (Steinhardt et al., 2014). Depth range based on vital effect
452 corrected $\delta^{18}\text{O}_{\text{CC}}$ of mid to large (adult) specimens of this species in our study shoal from eddy
453 condition (between 303 and 515 m with an average of 387 m) to non-eddy conditions (between
454 95 and 350 m with an average of 178 m). Thus, applying the 4°C offset to the $\delta^{18}\text{O}$ inferred
455 temperatures shifts calcification depth closer to those inferred from Mg/Ca for *G. scitula*. Both
456 Mg/Ca and $\delta^{18}\text{O}$ -derived calcification depth indicate a shoaling for this species. The range of
457 uncertainties related to a species' average calcification depth results from the relatively large
458 natural inter-specimen variability in Mg/Ca. Since we focus on relative differences within species
459 between hydrographic conditions, the uncertainty in calcification temperature resulting from
460 errors in the applied Mg/Ca-temperature calibration does not affect the absolute temperature
461 differences between the eddy- and non-eddy conditions. Instead, uncertainties in the calculated
462 difference in calcification depths between species will be caused by the inter-specimen variability
463 in Mg/Ca.

464

465 5.3.1 Cumulative calcification model

466 We used a conceptual oxygen isotope mass balance model (Wilke, 2006; 2009), applying the
467 temperature fractionation from inorganic calcite precipitation of Kim and O'Neil (1997) to our
468 measured $\delta^{18}\text{O}_{\text{CC}}$. The model equation describing foraminiferal migration as a function of depth
469 used here is known as the cumulative form of the Weibull function (Weibull, 1939). It is a
470 continuous probability function (Eq. 4), relating the shell mass 'M' to depth (z) using two
471 constants (α and β) determining the shape of this relationship:

472

$$473 \text{(4) } M(z) = 1 - \exp(-1 \cdot (z/\beta)^\alpha)$$

474

475 Since shell size of planktonic foraminifera is thought to increase with water depth (Hemleben
476 and Bijma, 1994; Peeters and Brummer, 2002) shell mass must also increase with depth. The
477 isotopic composition of a single shell thus represents the weighted sum of equilibrium calcite

478 precipitated over a depth range of the productive zone (i.e. where primary calcite formation takes
479 place).

480 Based on equation (5), the expected stable isotope composition of a specimen for a discrete
481 water depth interval can be calculated as follows:

482

483 (5)
$$\delta^{18}\text{O}_{\text{model}} = \sum_i^n \frac{(M_i - M_{i-1}) + \delta^{18}\text{O}_{\text{eq},i}}{M_i}$$

484

485 Given the $\delta^{18}\text{O}_{\text{eq}}$ profile in the water column and the measured $\delta^{18}\text{O}_{\text{cc}}$ of the planktonic
486 foraminifera it is possible to model the mass development (growth pattern) by using the
487 determined Mg/Ca calcification depth of the last chambers, indicating the base of the calcite
488 production zone. The Mg/Ca-based temperature of the F-1 chamber was used to delimit 95% of
489 the calcite production. In equation (5), $\delta^{18}\text{O}_{\text{eq},i}$ denotes the interval averaged $\delta^{18}\text{O}$ of equilibrium
490 calcite for the specified depth interval. For convenience, shell mass at the sea surface was taken
491 as zero and modelled $\delta^{18}\text{O}_{\text{cc}}$ was done by adapting the variables 'α' and 'β' in equation 5.

492 Increasing the value of 'α' results in a growth curve with a narrow calcification range. Higher
493 values for 'β' result in a deepening of the growth curve, thereby determining the position of the
494 base of the productive zone. In contrast to Wilke's (Wilke et al., 2006; 2009) approach, we have
495 determined the calcification temperatures of the last three to four chambers, which were used to
496 constrain the base of the calcification range and hence constrained values for 'β'.

497 In this model, it is assumed that shell growth always follows the same function, which is
498 continuous and does not differ between species. Offsets between $\delta^{18}\text{O}_{\text{CC}}$ and $\delta^{18}\text{O}_{\text{sw}}$ from
499 expected equilibrium ('the vital effect'), is assumed to be constant over the temperature range in
500 which the species calcifies. We have adapted $\delta^{18}\text{O}_{\text{sw}}$ in meter steps as calculated from *in situ*
501 salinity measurements, which were interpolated for the upper 2000 meters. We have used
502 expected $\delta^{18}\text{O}_{\text{eq}}$ values of eddy and non-eddy condition to compare depth distributions for all
503 four species of planktonic foraminifera.

504 Calcification depths inferred from the cumulative $\delta^{18}\text{O}$ model (Fig. 7) match previously published
505 calcification depths and associated temperatures for each of the species relatively well (e.g.
506 Cléroux et al., 2008; 2013; Wilke et al., 2009; Fallet et al., 2010; 2011; Birch et al., 2013). In three
507 species, measured $\delta^{18}\text{O}_{\text{CC}}$ values reflect shallower calcification depths than do single-chamber
508 Mg/Ca-based calcification depths, which is consistent with the general model of migration to
509 greater depth during growth. In case of the deep dwelling *G. scitula*, however, $\delta^{18}\text{O}$ -based
510 calcification depth is below that of the final chambers as derived from Mg/Ca-temperatures.
511 Without applying a temperature correction for $\delta^{18}\text{O}$ -based calcification temperatures of *G.*

512 *scitula*, calcification depth based on $\delta^{18}\text{O}_{\text{CC}}$ can deviate up to 300 m from the Mg/Ca based
513 depths. This would suggest that the majority of the previously formed calcite was precipitated
514 deeper in the water column. For our calcification model we corrected $\delta^{18}\text{O}_{\text{CC}}$ for the vital effect
515 (Kahn and Williams, 1981). The model shows that species modulate their calcification pattern
516 depending on the hydrographical conditions they live in (e.g. eddy, non-eddy condition). For *G.*
517 *ruber*, our results show that this species seems to be an exclusive surface dweller and hence an
518 application of the cumulative calcification model only confirms that the majority of the calcite is
519 formed at the sea surface.

520 For the thermocline dwelling species *N. dutertrei* we find that this species calcifies most of its
521 calcite in a narrow depth range. Our model indicates that calcification during eddy conditions is
522 more intense in the deeper part of the thermocline ($\alpha= 8.8$; $\beta= 85$), whereas calcification during
523 non-eddy condition is more equally distributed over the entire thermocline ($\alpha= 1.9$; $\beta= 47$). It is
524 noteworthy that *N. dutertrei* appears to intensify its calcification efforts during eddy conditions
525 deeper in the thermocline, matching well with the deepening of the isopycnals and hence a
526 narrower range of optimal calcification conditions (Steinhardt et al., 2014). This calcification
527 response is also reflected in more enriched $\delta^{13}\text{C}$ values during eddy conditions. For *P.*
528 *obliquiloculata* modelled α and β values are relatively high, particularly during eddy conditions
529 ($\alpha= 5.25$; $\beta= 133$, compared to $\alpha= 3.1$; $\beta= 63$ for non-eddy conditions). This indicates that most
530 of the calcification in *P. obliquiloculata* takes place at a water depth around 125 m during eddy
531 conditions, and around 50 m during non-eddy conditions. The range at which *G. scitula* calcifies
532 is well below the seasonal thermocline, reflected by high values for α and β (Fig. 7) and does not
533 vary considerably during eddy and non-eddy conditions.

534 In general, we conclude that temperature changes within the thermocline induced by eddies
535 affect non-symbiotic species mostly. Also, changes in cumulative calcite addition with depth
536 seem to be species-specific. We modified the model by including Mg/Ca-based temperatures
537 (following the species specific equations of Anand et al., 2003) of the F-1 chamber to constrain
538 the 95% calcification level. This allows to predict expected $\delta^{18}\text{O}_{\text{eq}}$ for different species and shell
539 sizes (Spero et al., 1997; Bijma et al., 1999; Itou et al., 2001; Peeters et al., 2002). The
540 extended version of the model does not distinguish between calcite deposited during chamber
541 formation (primary calcite) and calcite added as a result of wall thickening due to gametogenic
542 calcite or the precipitation of crust (secondary calcite, Bé, 1980; Duplessy et al., 1981; Lohmann,
543 1995, Jonkers et al., 2012). Secondary calcification might play an important role for deeper
544 dwelling species such as *G. scitula*, which could explain the offset (0.48‰) between $\delta^{18}\text{O}_{\text{model}}$
545 and $\delta^{18}\text{O}_{\text{CC}}$ during non-eddy conditions. This suggests that relatively more calcite is formed

546 deeper in the water column, or secondary calcite is precipitated with a fundamentally different
547 calcification mechanism.

548

549 **5.3.2 Carbon isotopes – testing the calcification model**

550 The $\delta^{13}\text{C}$ values found in planktonic foraminifera is primarily a function of the carbon isotope
551 composition of the dissolved inorganic carbon (DIC) in seawater (e.g. Urey, 1947; Epstein et al.,
552 1953; McCorkle et al., 1990), which changes with water depth (e.g. Fairbanks et al., 1980, Curry
553 and Crowley, 1987). Therefore, we can use the cumulative mass balance model output of the
554 mass added per meter to calculate $\delta^{13}\text{C}_{\text{expect}}$ as the weighted sum of the $\delta^{13}\text{C}_{\text{DIC}}$ (Wilke et al.,
555 2006). Depth-resolved carbon isotope composition ($\delta^{13}\text{C}_{\text{DIC}}$), available from locations closest to
556 our study site (locations between 37-43 °E and 24.7 °S, World Ocean Database 2009) were
557 used to calculate the expected $\delta^{13}\text{C}$ of each species of foraminifera ($\delta^{13}\text{C}_{\text{expect}}$). Since there is no
558 relation between size and stable carbon isotopes in our specimens, the employed size fractions
559 contained only mature (adult) specimens (Brummer et al., 1986, 1987). Comparing water column
560 $\delta^{13}\text{C}_{\text{DIC}}$ data (Supplement, Fig. A1) from several stations near the MC reveals that absolute
561 values and depth range over which values decrease is similar at the different sites. To verify the
562 depth related calcification model we compare measured $\delta^{13}\text{C}_{\text{CC}}$ with model-based $\delta^{13}\text{C}_{\text{expect}}$
563 values (Fig. 8).

564 Carbon isotope values become more negative from surface dwelling *G. ruber* towards deeper
565 dwelling *P. obliquiloculata* near the upper thermocline. Conversely, the $\delta^{13}\text{C}$ of *Globorotalia*
566 *scitula* increases with depth. Low temperatures and reduced food availability have been
567 suggested to result in relatively low metabolic rates in deep dwelling species, so that their $\delta^{13}\text{C}$
568 likely approaches $\delta^{13}\text{C}_{\text{DIC}}$ values (Birch et al., 2013). This suggests the involvement of biological
569 controls on the $\delta^{13}\text{C}$ of the different genera (*Globigerinoides*, *Neogloboquadrina*, *Pulleniatina*
570 and *Globorotalia*). All $\delta^{13}\text{C}_{\text{expect}}$ are higher than the measured $\delta^{13}\text{C}_{\text{CC}}$.

571 Our cumulative mass balance shows that the majority of the carbonate of *G. ruber* is formed in
572 surface waters (Fig. 7). Equal $\delta^{13}\text{C}_{\text{expect}}$ values for eddy and non-eddy conditions are the result of
573 similarly enriched $\delta^{13}\text{C}_{\text{DIC}}$ in the mixed layer. The measured differences in $\delta^{13}\text{C}_{\text{CC}}$ (Fig. 8) are
574 likely a consequence of the deepening thermocline during passage of an eddy, carrying nutrient-
575 depleted waters (Kolasinski et al., 2013). Anticyclonic eddies are characterized by accumulation
576 of warm, nutrient-poor and chlorophyll-depleted water in the center, which implies that also
577 $\delta^{13}\text{C}_{\text{DIC}}$ is more isotopically enriched. Still, local nutrient enrichment potentially occurs at the
578 outer edge as a result of high turbulence along the isopycnal slope (e.g. Falkowski et al., 1991;

579 Lévy, 2003). The strong response of the Mg/Ca and $\delta^{18}\text{O}$ of *N. dutertrei* during eddy conditions
580 (deeper calcification) is also reflected by more depleted $\delta^{13}\text{C}_{\text{CC}}$ values. Remineralization of
581 organic matter at greater depth cause enrichment of $\delta^{13}\text{C}_{\text{DIC}}$, resulting in the incorporation of
582 lighter carbon isotopes into the shell of *N. dutertrei* during eddy conditions. Based on samples
583 from a sediment trap in Cape basin, Wilke et al. (2009) showed that the species *N. dutertrei* is
584 an accurate recorder of the $\delta^{13}\text{C}_{\text{DIC}}$. This is in agreement with previous findings (Mulitza et al.,
585 1999), showing that the carbon isotopic composition of *N. dutertrei* exhibits a constant and
586 temperature-independent off-set from $\delta^{13}\text{C}_{\text{DIC}}$ of $\sim 0.5\text{‰}$ over a wide temperature range. This
587 difference is in line with the offset in our dataset between $\delta^{13}\text{C}_{\text{expect}}$ and $\delta^{13}\text{C}_{\text{CC}}$ of *N. dutertrei*
588 (0.6‰).

589 The $\delta^{13}\text{C}$ of the symbiont-barren *G. scitula* significantly deviates from those of the shallower
590 dwelling species as a result of a decrease in $\delta^{13}\text{C}_{\text{DIC}}$ with water depth (see supplementary
591 information, Fig. A1 and A2). The more depleted $\delta^{13}\text{C}_{\text{CC}}$ of *G. scitula* may also be a
592 consequence of a lower metabolism of this species (Vergnaud-Grazzini, 1976; Kahn, 1977,
593 1979; Berger et al, 1978; Erez, 1978) compared to that of *G. ruber* and *N. dutertrei*. At high
594 metabolic activity, more isotopically lighter carbon is incorporated and since lower temperatures
595 usually reduce metabolic rates, species inhabiting deeper water depths may incorporate
596 relatively heavier carbon isotopes. Minor changes in $\delta^{13}\text{C}_{\text{CC}}$ for *G. scitula* during eddy versus non-
597 eddy conditions are in line with the minor response in calcification depth for this species. Similar
598 to previous conclusions, this suggests that Mg/Ca inferred temperature differences between *N.*
599 *dutertrei* and *G. scitula* are good indicators for eddies passing (Steinhardt et al., 2014). In
600 addition, the $\delta^{13}\text{C}_{\text{CC}}$ differences between these species might very well help to reconstruct eddy
601 frequency in this area. The depth integrated difference between $\delta^{13}\text{C}$ of *N. dutertrei* and *G.*
602 *scitula* changes from 0.25 to 0.05 ‰.

603 Comparing $\delta^{13}\text{C}_{\text{expect}}$ and $\delta^{13}\text{C}_{\text{CC}}$ for *P. obliquiloculata* there is a discrepancy between eddy and
604 non-eddy conditions (Fig. 8). Similar to *N. dutertrei*, this species is mostly associated with the
605 thermocline (Anand et al., 2003; Cléroux et al., 2008; Sadekov et al., 2009). Our cumulative
606 calcification model showed a slightly deeper calcification depth for *N. dutertrei* and a minor eddy
607 response in calcification range (Fig. 7). However, $\delta^{13}\text{C}$ values indicate a significant difference
608 between eddy and non-eddy conditions. Mulitza et al. (1999) showed that *P. obliquiloculata* does
609 not calcify in isotopic equilibrium with dissolved ΣCO_2 , but the deviation from isotopic equilibrium
610 is a linear function of temperature (Fig. 8). While the mean of the $\delta^{13}\text{C}$ cannot be used to infer
611 the actual calcification depth, they argue that the spread and skewness of the individual $\delta^{13}\text{C}$

612 measurements should still be representative of the range of calcification depths and habitat
613 preferences within the thermocline.

614 Also changes in the carbonate ion concentration with depth potentially play an important role in
615 the observed differences between species and between eddy and non-eddy conditions
616 (supplementary, Fig. A1 and A2). Since the carbonate ion profile is expected to change in
617 accordance with thermocline deepening when an eddy passes we refrained from correcting for
618 this. The observed offsets between species, however, suggest that carbonate ion does play a
619 role there. The deeper living species show an increasing offset with respect to the 1:1 line (Fig.
620 8). The exception is *P. obliquiloculata* which responds to temperature rather than $\delta^{13}\text{C}_{\text{DIC}}$
621 carbonate ion changes (Mulitza et al., 1999).

622 Overall the here observed relations indicate that interpretation of the foraminifera vertical
623 distribution in the upper water column can be unraveled by coupling various geochemical
624 methods in order to retrieve calcification temperature at different stages in a foraminifera's life
625 cycle. This in turn can be used to develop new proxies for the thermal and nutrient structure of
626 the upper part of the water column.

627

628 **6. Conclusion**

629 Documenting changes in upper ocean stratification is essential for understanding past climatic
630 conditions from sediment cores and is commonly estimated by determining the difference in
631 $\delta^{18}\text{O}$ between thermocline and surface-dwelling planktonic foraminifera (Spero et al., 2003;
632 Cléroux et al., 2007; Farmer et al., 2007; Lin and Hsieh, 2007; Steph et al., 2009). We
633 conducted stable isotope measurements on four species of planktonic foraminifera (*G. ruber*, *N.*
634 *dutertrei*, *P. obliquiloculata* and *G. scitula*) from selected sediment trap samples, representing
635 eddy and non-eddy conditions in the MC.

636 Using single shell $\delta^{18}\text{O}_{\text{CC}}$ paired to single-chamber LA-ICP-MS Mg/Ca measurements we
637 applied a cumulative mass balance model in order to compare growth patterns of the various
638 planktonic species during eddy and non-eddy conditions. The results indicate that most of the
639 species have somewhat different calcification patterns during eddy and non-eddy conditions.
640 Only Mg/Ca values of *G. scitula* suggest higher calcification temperatures than inferred from
641 $\delta^{18}\text{O}$. Furthermore, the results of the $\delta^{18}\text{O}$ cumulative mass balance model agree with previous
642 findings that thermocline dwelling *N. dutertrei* and deep dwelling *G. scitula* are suitable recorders
643 of eddy induced hydrographic changes (Steinhardt et al., 2014). The combination of various

644 proxies (e.g. Mg/Ca, $\delta^{18}\text{O}$ and $\delta^{13}\text{C}$) can thus provide a useful set of geochemical proxies to
645 reconstruct the thermal and nutrient structure of the upper part of the water column.

646
647 All species analyzed have unique offsets from ambient seawater $\delta^{13}\text{C}$. However, comparison of
648 species specific isotopic trajectories with water column $\delta^{13}\text{C}$ reveals that ambient $\delta^{13}\text{C}_{\text{DIC}}$ may be
649 recorded by the species used in this study. The $\delta^{13}\text{C}$ of *N. dutertrei* and *G. scitula* show eddy
650 related changes in their offsets and can potentially aid to unravel eddy related changes in the
651 nutrient structure.

652

653 **The Supplement related to this article is available online at**
654 **doi:10.5194/bgd-11-17255-2014-supplement.**

655

656 *Acknowledgements.* We acknowledge funding from the European Commission 7th Framework Marie
657 Curie People program FP7/2007–2013 through funding of the Initial Training Network “GATEWAYS”
658 (<http://www.gateways-itn.eu>) under the grant number 238512. Furthermore we acknowledge funding from
659 the LOCO and INATEX programs by the Netherlands Organisation for Scientific Research. Analyses and
660 visualizations of satellite SST used in this paper were produced with the Giovanni online data system,
661 developed and maintained by the NASA GES DISC. We thank the chief scientist Herman Ridderinkhof
662 and the crew of the RRV Charles Darwin, RRV Discovery, FS Meteor, RV Pelagia and R/V Algoa. Great
663 thanks to Helen de Waard and Michiel Kienhuis for providing technical support with the trace element
664 analysis at Utrecht University and Suzanne Verdegaal for supporting the measurements at the Vrije
665 Universiteit Amsterdam.

666

667 **References:**

668

669 Anand, P., Elderfield, H. and Conte, M.: Calibration of Mg/Ca thermometry in planktonic foraminifera from
670 a sediment trap time series, *Paleoceanography*, 18, 28–31, 2003.

671 Anand, P., Kroon, D., Singh, A., Ganeshram, R., Ganssen, G., and Elderfield, H.: Coupled sea surface
672 temperature–seawater $\delta^{18}\text{O}$ reconstructions in the Arabian Sea at the millennial scale for the last 35 ka,
673 *Paleoceanography*, 23, PA4207, doi: 10.1029/2007PA001564, 2008.

674 Backeberg, B. and Reason, C.: A connection between the South Equatorial Current north of Madagascar
675 and Mozambique Channel Eddies, *Geophys. Res. Lett.*, 37, L04604, doi: 10.1029/2009GL041950, 2010.

676 Barker, S., Greaves, M. and Elderfield, H.: A study of cleaning procedures used for foraminiferal Mg/Ca
677 paleothermometry, *Geochem. Geophys. Geosystems*, 4, 8407, 2003.

678 Bé, A. W.: Planktonic foraminifera, *Antarct. Map Folio Ser. Am. Geogr. Soc.*, 9–12, 1969.

679 Bé, A. W. H.: An ecological, zoogeographic and taxonomic review of recent planktonic foraminifera,
680 *Ocean. Micropalaeontology*, 1, 305–316, 1977.

681 Bé, A. W., Hemleben, C., Anderson, O. R. and Spindler, M.: Chamber formation in planktonic foraminifera,
682 *Micropaleontology*, 25, 294–307, 1979.

683 Bé, A. W. H.: Gametogenic calcification in a spinose planktonic foraminifer, *Globigerinoides sacculifer*
684 (Brady), *Mar. Micropaleontol.*, 5, 283–310, doi:10.1016/0377-8398(80)90014-6, 1980.

685 Bé, A. W. and Spero, H. J.: Shell regeneration and biological recovery of planktonic foraminifera after
686 physical injury induced in laboratory culture, *Micropaleontology*, 27, 305–316, 1981.

687 Bemis, B. E., Spero, H. J., Bijma, J. and Lea, D. W.: Reevaluation of the oxygen isotopic composition of
688 planktonic foraminifera: Experimental results and revised paleotemperature equations,
689 *Paleoceanography*, 13(2), 150–160, doi:10.1029/98PA00070, 1998.

690 Berger, W., Killingley, J. and Vincent, E.: Sable isotopes in deep-sea carbonates-box core erdc-92, west
691 equatorial pacific, *Oceanol. Acta*, 1, 203–216, 1978.

692 Bijma, J., Spero, H. and Lea, D.: Reassessing foraminiferal stable isotope geochemistry: Impact of the
693 oceanic carbonate system (experimental results), in *Use of proxies in paleoceanography*, pp. 489–512,
694 Springer, Berlin Heidelberg, 1999.

695 Birch, H., Coxall, H. K., Pearson, P. N., Kroon, D. and O'Regan, M.: Planktonic foraminifera stable
696 isotopes and water column structure: Disentangling ecological signals, *Mar. Micropaleontol.*, 10, 127-145,
697 2013.

698 Brady, H.: Foraminifera in Tizard and Murray's Exploration of the Faroe Channel, vol. 11. In *Proc. Roy.*
699 *Soc*, 1882.

700 Brady, H.: Foraminifera in Tizard and Murray's Exploration of the Faroe Channel, vol. 11. 1882.

701 Brummer, G.-J. A., Hemleben, C. and Spindler, M.: Planktonic foraminiferal ontogeny and new
702 perspectives for micropalaeontology, *Nature*, 319(6048), 50–52, doi:10.1038/319050a0, 1986.

703 Brummer, G.-J. A., Hemleben, C. and Spindler, M.: Ontogeny of extant spinose planktonic foraminifera
704 (*Globigerinidae*): A concept exemplified by *Globigerinoides sacculifer* (Brady) and *G. ruber* (d'Orbigny),
705 *Mar. Micropaleontol.*, 12, 357–381, doi:10.1016/0377-8398(87)90028-4, 1987.

706 Cléroux, C., Cortijo, E., Duplessy, J. and Zahn, R.: Deep-dwelling foraminifera as thermocline temperature
707 recorders, *Geochem. Geophys. Geosystems*, 8, 2007.

708 Cléroux, C., Cortijo, E., Anand, P., Labeyrie, L., Bassinot, F., Caillon, N. and Duplessy, J.-C.: Mg/Ca and
709 Sr/Ca ratios in planktonic foraminifera: Proxies for upper water column temperature reconstruction,
710 *Paleoceanography*, 23, PA3214, doi: 10.1029/2007pa001505, 2008.

711 Cléroux, C., deMenocal, P., Arbuszewski, J. and Linsley, B.: Reconstructing the upper water column
712 thermal structure in the Atlantic Ocean, *Paleoceanography*, 28(3), 503–516, doi: 10.1002/palo.20050,
713 2013.

714 Curry, W. B. and Crowley, T. J.: The $\delta^{13}\text{C}$ of equatorial Atlantic surface waters: Implications for ice age
715 pCO₂ levels, *Paleoceanography*, 2, 489–517, 1987.

716 Curry, W. B., Thunell, R. C. and Honjo, S.: Seasonal changes in the isotopic composition of planktonic
717 foraminifera collected in Panama Basin sediment traps, *Earth Planet. Sci. Lett.*, 64, 33–43, doi:
718 10.1016/0012-821X(83)90050-X, 1983.

719 Damassa, T. D., Cole, J. E., Barnett, H. R., Ault, T. R. and McClanahan, T. R.: Enhanced multidecadal
720 climate variability in the seventeenth century from coral isotope records in the western Indian Ocean,
721 *Paleoceanography*, 21, PA2016, doi: 10.1029/2005PA001217, 2006.

722 Deuser, W. G.: Variability of hydrography and particle flux: Transient and long-term relationships, *Mitt.*
723 *Geol.-Palaeont. Inst. Univ. Hambg.*, 62, 179–193, 1987.

724 Deuser, W. G. and Ross, E. H.: Seasonally abundant planktonic foraminifera of the Sargasso Sea;
725 succession, deep-water fluxes, isotopic compositions, and paleoceanographic implications, *J. Foraminifer.*
726 *Res.*, 19, 268–293, doi: 10.2113/gsjfr.19.4.268, 1989.

727 Deuser, W., Ross, E., Hemleben, C. and Spindler, M.: Seasonal changes in species composition,
728 numbers, mass, size, and isotopic composition of planktonic foraminifera settling into the deep Sargasso
729 Sea, *Palaeogeogr. Palaeoclimatol. Palaeoecol.*, 33, 103–127, 1981.

730 Duplessy, J. C., Bé, A. W. H. and Blanc, P. L.: Oxygen and carbon isotopic composition and
731 biogeographic distribution of planktonic foraminifera in the Indian Ocean, *Palaeogeogr. Palaeoclimatol.*
732 *Palaeoecol.*, 33, 9–46, doi: 10.1016/0031-0182(81)90031-6, 1981.

733 Durgadoo, J.V., Loveday, B.R., Reason, C.J., Penven, P., Biastoch, A.: Agulhas leakage predominantly
734 responds to the Southern Hemisphere Westerlies. *J. Phys. Oceanogr.* 43, 2113–2131.
735 <http://dx.DOI.org/10.1175/JPO-D-13-047.1>, 2013

736 Eggins, S., De Deckker, P. and Marshall, J.: Mg/Ca variation in planktonic foraminifera tests: Implications
737 for reconstructing palaeo-seawater temperature and habitat migration, *Earth Planet. Sci. Lett.*, 212, 291–
738 306, 2003.

739 Eguchi, N. O., Ujiie, H., Kawahata, H. and Taira, A.: Seasonal variations in planktonic foraminifera at three
740 sediment traps in the subarctic, transition and subtropical zones of the central North Pacific Ocean, *Mar.*
741 *Micropaleontol.*, 48, 149–163, 2003.

742 Elderfield, H., Bertram, C. J. and Erez, J.: A biomineralization model for the incorporation of trace
743 elements into foraminiferal calcium carbonate, *Earth Planet. Sci. Lett.*, 142, 409–423, doi: 10.1016/0012-
744 821X(96)00105-7, 1996.

745 Elderfield, H. and Ganssen, G.: Past temperature and ^{18}O of surface ocean waters inferred from
746 foraminiferal Mg/Ca ratios, *Nature*, 405, 442–445, 2000.

747 Emiliani, C.: Depth habitats of some species of pelagic Foraminifera as indicated by oxygen isotope ratios,
748 *Am. J. Sci.*, 252, 149–158, doi: 10.2475/ajs.252.3.149, 1954.

749 Epstein, S. and Mayeda, T.: Variation of O^{18} content of waters from natural sources, *Geochim.*
750 *Cosmochim. Acta*, 4, 213–224, 1953.

751 Erez, J.: Vital effect on stable-isotope composition seen in foraminifera and coral skeletons, *Nature* 273,
752 199–202, doi:10.1038/273199a0, 1978.

753 Erez, J.: The source of ions for biomineralization in foraminifera and their implications for
754 paleoceanographic proxies, *Rev. Mineral. Geochem.*, 54, 115–149, 2003.

755 Erez, J. and Honjo, S.: Comparison of isotopic composition of planktonic foraminifera in plankton tows,
756 sediment traps and sediments, *Palaeogeogr. Palaeoclimatol. Palaeoecol.*, 33, 129–156,
757 doi:10.1016/0031-0182(81)90035-3, 1981.

758 Fairbanks, R. G., Wiebe, P. H. and Bé, A. W.: Vertical distribution and isotopic composition of living
759 planktonic foraminifera in the western North Atlantic, *Science*, 207, 61–63, 1980.

760 Fairbanks, R. G., Sverdrlove, M., Free, R., Wiebe, P. H. and Bé, A. W.: Vertical distribution and isotopic
761 fractionation of living planktonic foraminifera from the Panama Basin, *Nature*, 298, 841–844, 1982.

762 Falkowski, P. G., Ziemann, D., Kolber, Z. and Bienfang, P. K.: Role of eddy pumping in enhancing primary
763 production in the ocean, *Nature* 352, 55-58, doi:10.1038/352055a0, 1991.

764 Fallet, U., Boer, W., van Assen, C., Greaves, M. and Brummer, G.-J. A.: A novel application of wet
765 oxidation to retrieve carbonates from large organic-rich samples for ocean-climate research, *Geochem*
766 *Geophys Geosyst*, 10, Q08004, doi: 10.1029/2009gc002573, 2009.

767 Fallet, U., Brummer, G.-J., Zinke, J., Vogels, S. and Ridderinkhof, H.: Contrasting seasonal fluxes of
768 planktonic foraminifera and impacts on paleothermometry in the Mozambique Channel upstream of the
769 Agulhas Current, *Paleoceanography*, 25, PA4223, doi: 10.1029/2010pa001942, 2010.

770 Fallet, U., Ullgren, J. E., Castañeda, I. S., van Aken, H. M., Schouten, S., Ridderinkhof, H. and Brummer,
771 G.-J. A.: Contrasting variability in foraminiferal and organic paleotemperature proxies in sedimenting
772 particles of the Mozambique Channel (SW Indian Ocean), *Geochim. Cosmochim. Acta*, 75, 5834–5848,
773 2011.

774 Fallet, U., Castañeda, I. S., Henry-Edwards, A., Richter, T. O., Boer, W., Schouten, S. and Brummer, G.-
775 J.: Sedimentation and burial of organic and inorganic temperature proxies in the Mozambique Channel,
776 SW Indian Ocean, *Deep Sea Res. Part Oceanogr. Res. Pap.*, 59, 37–53, 2012.

777 Farmer, E. C., Kaplan, A., de Menocal, P. B. and Lynch-Stieglitz, J.: Corroborating ecological depth
778 preferences of planktonic foraminifera in the tropical Atlantic with the stable oxygen isotope ratios of core
779 top specimens, *Paleoceanography*, 22(3), doi:DOI: 10.1029/2006PA001361, 2007.

780 Faul, K. L., Ravelo, A. C. and Delaney, M. L.: Reconstructions of Upwelling, Productivity, and Photic Zone
781 Depth in the Eastern Equatorial Pacific Ocean Using Planktonic Foraminiferal Stable Isotopes and
782 Abundances, *J. Foraminifer. Res.*, 30, 110–125, doi: 10.2113/0300110, 2000.

783 Field, D. B.: Variability in vertical distributions of planktonic foraminifera in the California Current:
784 Relationships to Vertical Ocean structure, *Paleoceanography*, 19, PA2014, doi:10.1029/2003PA000970,
785 2004.

786 Friedrich, O., Schiebel, R., Wilson, P. A., Weldeab, S., Beer, C. J., Cooper, M. J. and Fiebig, J.: Influence
787 of test size, water depth, and ecology on Mg/Ca, Sr/Ca, $\delta^{18}\text{O}$ and $\delta^{13}\text{C}$ in nine modern species of planktic
788 foraminifers, *Earth Planet. Sci. Lett.*, 319, 133–145, doi: 10.1016/j.epsl.2011.12.002, 2012.

789 Ganssen, G. and Sarnthein, M.: Stable-Isotope Composition of Foraminifers: The Surface and Bottom
790 Water Record of Coastal Upwelling, in *Coastal Upwelling Its Sediment Record*, edited by E. Suess and J.
791 Thiede, pp. 99–121, Springer US. [online] Available from: http://link.springer.com/chapter/10.1007/978-1-4615-6651-9_6 (Accessed 5 December 2013), 1983.

793 Grossman, E. L.: Stable isotopes in modern benthic foraminifera; a study of vital effect, *J. Foraminifer.*
794 *Res.*, 17, 48–61, 1987.

795 Gründlingh, M. L.: Tracking eddies in the southeast Atlantic and southwest Indian oceans with
796 TOPEX/POSEIDON, *J. Geophys. Res.*, 100, 24977–24,986, 1995.

797 Hastenrath, S., Nicklis, A. and Greischar, L.: Atmospheric-hydrospheric mechanisms of climate anomalies
798 in the western equatorial Indian Ocean, *J. Geophys. Res. Oceans*, 98, 20219–20235, doi:
799 10.1029/93JC02330, 1993.

800 Hathorne, E. C., James, R. H. and Lampitt, R. S.: Environmental versus biomineralization controls on the
801 intratest variation in the trace element composition of the planktonic foraminifera *G. inflata* and *G. scitula*,
802 *Paleoceanography*, 24, PA4204, doi: 10.1029/2009pa001742, 2009.

803 Hemleben, C. and Bijma, J.: Foraminiferal population dynamics and stable carbon isotopes, in *Carbon*
804 *Cycling in the Glacial Ocean: Constraints on the Ocean's Role in Global Change*, Springer, Berlin
805 Heidelberg, 145–166, 1994.

806 Hemleben, C., Spindler, M. and Anderson, O.: *Modern planktonic foraminifera*, Springer, Berlin, 363 pp.,
807 1989.

808 Huang, K., You, C., Lin, H. and Shieh, Y.: In situ calibration of Mg/Ca ratio in planktonic foraminiferal shell
809 using time series sediment trap: A case study of intense dissolution artifact in the South China Sea,
810 *Geochem. Geophys. Geosystems*, 9, Q04016, doi:10.1029/207GC001660, 2008.

811 Hut, G.: *Stable Isotope Reference Samples for Geochemical and Hydrological Investigations*. Rep. to Dir.
812 Gen., International Atomic Energy Agency, Vienna, 42 pp., 1987.

813 Itou, M., Ono, T., Oba, T. and Noriki, S.: Isotopic composition and morphology of living *Globorotalia*
814 *scitula*: a new proxy of sub-intermediate ocean carbonate chemistry?, *Mar. Micropaleontol.*, 42, 189–210,
815 2001.

816 Jonkers, L., de Nooijer, L., Reichart, G., Zahn, R. and Brummer, G.: Encrustation and trace element
817 composition of *Neogloboquadrina dutertrei* assessed from single chamber analyses, implications for
818 paleotemperature estimates, *Biogeosciences*, 9, 4851–4860, doi:10.5194/bg-9-4851-2012, 2012.

819 Kahn, M. I.: Non-equilibrium oxygen and carbon isotopic fractionation in tests of living planktic foraminifera
820 from the eastern equatorial Atlantic Ocean, Ph.D. thesis, University of South California, Los Angeles, 224
821 p., 1977.

822 Kahn, M.: Non-equilibrium oxygen and carbon isotopic fractionation in tests of living planktonic-
823 foraminifera, *Oceanol. Acta*, 2, 195–208, 1979.

824 Kahn, M. I. and Williams, D. F.: Oxygen and carbon isotopic composition of living planktonic foraminifera
825 from the northeast Pacific Ocean, *Palaeogeogr. Palaeoclimatol. Palaeoecol.*, 33, 47–69, 1981.

826 Kiefer, T., McCave, I. N. and Elderfield, H.: Antarctic control on tropical Indian Ocean sea surface
827 temperature and hydrography, *Geophys. Res. Lett.*, 33, L24612, doi:10.1029/2006GL027097, 2006.

828 Kim, S.-T. and O'Neil, J. R.: Equilibrium and nonequilibrium oxygen isotope effects in synthetic
829 carbonates, *Geochim. Cosmochim. Acta*, 61, 3461–3475, doi: 10.1016/S0016-7037(97)00169-5, 1997.

830 Kolasinski, J., Kaehler, S. and Jaquemet, S.: Distribution and sources of particulate organic matter in a
831 mesoscale eddy dipole in the Mozambique Channel (south-western Indian Ocean): Insight from C and N
832 stable isotopes, *J. Mar. Syst.*, 96-97, 122-131, doi:10.1016/j.jmarsys.2012.02.015, 2012.

833 Kroon, D. and Darling, K.: Size and upwelling control of the stable isotope composition of
834 *Neogloboquadrina dutertrei* (d'Orbigny), *Globigerinoides ruber* (d'Orbigny) and *Globigerina bulloides*
835 d'Orbigny; examples from the Panama Basin and Arabian Sea, *J. Foraminifer. Res.*, 25, 39–52, 1995.

836 Kunioka, D., Shirai, K., Takahata, N., Sano, Y., Toyofuku, T. and Ujiie, Y.: Microdistribution of Mg/Ca,
837 Sr/Ca, and Ba/Ca ratios in *Pulleniatina obliquiloculata* test by using a NanoSIMS: Implication for the vital
838 effect mechanism, *Geochem. Geophys. Geosystems*, 7, Q12P20, doi:10.1029/2006GC001280, 2006.

839 Kuroyanagi, A. and Kawahata, H.: Vertical distribution of living planktonic foraminifera in the seas around
840 Japan, *Mar. Micropaleontol.*, 53, 173–196, doi: 10.1016/j.marmicro.2004.06.001, 2004.

841 Lévy, M.: Mesoscale variability of phytoplankton and of new production: Impact of the large-scale nutrient
842 distribution, *J. Geophys. Res. Oceans* 1978–2012, 108, 3358, doi:10.1029/2002JC001577, 2003.

843 Lin, H.-L. and Hsieh, H.-Y.: Seasonal variations of modern planktonic foraminifera in the South China Sea,
844 *Deep Sea Res. Part II Top. Stud. Oceanogr.*, 54, 1634–1644, 2007.

845 Lohmann, G. P.: A model for variation in the chemistry of planktonic foraminifera due to secondary
846 calcification and selective dissolution, *Paleoceanography*, 10(3), 445–457, doi:10.1029/95PA00059, 1995.

847 Lončarić, N., van Iperen, J., Kroon, D. and Brummer, G.-J. A.: Seasonal export and sediment preservation
848 of diatomaceous, foraminiferal and organic matter mass fluxes in a trophic gradient across the SE Atlantic,
849 *Prog. Oceanogr.*, 73, 27–59, 2007.

850 Lončarić, N., Peeters, F. J. C., Kroon, D. and Brummer, G. J. A.: Oxygen isotope ecology of recent
851 planktic foraminifera at the central Walvis Ridge (SE Atlantic), *Paleoceanography*, 21, 3009, 2006.

852 McClanahan, T. R.: Seasonality in East Africa's coastal waters., *Mar. Ecol. Prog. Ser. Oldendorf*, 44, 191–
853 199, 1988.

854 McCorkle, D. C., Keigwin, L. D., Corliss, B. H. and Emerson, S. R.: The influence of microhabitats on the
855 carbon isotopic composition of deep-sea benthic foraminifera, *Paleoceanography*, 5, 161–185, 1990.

856 Mohtadi, M., Hebbeln, D., Nuñez Ricardo, S. and Lange, C. B.: El Niño-like pattern in the Pacific during
857 marine isotope stages (MIS) 13 and 11?, *Paleoceanography*, 21, PA1015, doi:10.1029/2005PA001190,
858 2006.

859 Mulitza, S., Dürkoop, A., Hale, W., Wefer, G. and Niebler, H. S.: Planktonic foraminifera as recorders of
860 past surface-water stratification, *Geology*, 25, 335–338, doi: 10.1130/0091-7613, 1997.

861 Mulitza, S., Arz, H., Kemle-von Mücke, S., Moos, C., Niebler, H.-S., Pätzold, J. and Segl, M.: The South
862 Atlantic carbon isotope record of planktic foraminifera, in *Use of Proxies in Paleoceanography*, pp. 427–
863 445, Springer., 1999.

864 New, A., Alderson, S., Smeed, D. and Stansfield, K.: On the circulation of water masses across the
865 Mascarene Plateau in the South Indian Ocean, *Deep Sea Res. Part Oceanogr. Res. Pap.*, 54, 42–74,
866 2007.

867 Oppo, D. W. and Fairbanks, R. G.: Carbon isotope composition of tropical surface water during the past
868 22,000 years, *Paleoceanography*, 4, 333–351, 1989.

869 D'Orbigny, A.: Foraminifères, *Hist. Phys. Polit. Nat. Lî Cuba Bertrand Paris*, 1839.

870 Ortiz, J., Mix, A., Rugh, W., Watkins, J. and Collier, R.: Deep-dwelling planktonic foraminifera of the
871 northeastern Pacific Ocean reveal environmental control of oxygen and carbon isotopic disequilibria,
872 *Geochim. Cosmochim. Acta*, 60, 4509–4523, 1996.

873 Patrick, A. and Thunell, R. C.: Tropical Pacific sea surface temperatures and upper water column thermal
874 structure during the last glacial maximum, *Paleoceanography*, 12, 649–657, 1997.

875 Parker, W. K., Jones, T. R., Bailey, J. and Pourtales, F.: On some foraminifera from the north Atlantic and
876 Arctic Oceans, including Davis Straits and Baffin's Bay, *Philos. Trans. R. Soc. Lond.*, 155, 325–441, 1865.

877 Peeters, F. J. C. and Brummer, G.-J. A.: The seasonal and vertical distribution of living planktic
878 foraminifera in the NW Arabian Sea, *Geol. Soc. Lond. Spec. Publ.*, 195, 463–497, doi:
879 10.1144/GSL.SP.2002.195.01.26, 2002

880 Peeters, F., Brummer, G. and Ganssen, G.: The effect of upwelling on the distribution and stable isotope
881 composition of *Globigerina bulloides* and *Globigerinoides ruber* (planktic foraminifera) in modern surface
882 waters of the NW Arabian Sea, *Glob. Planet. Change*, 34, 269–291, 2002.

883 Ravelo, A. and Fairbanks, R.: Oxygen isotopic composition of multiple species of planktonic foraminifera:
884 Records of the modern photic zone temperature gradient, *Paleoceanography*, 7, 815–831, 1992.

885 Ravelo, A. and Fairbanks, R.: Carbon isotopic fractionation in multiple species of planktonic foraminifera
886 from core-tops in the tropical Atlantic, *J. Foraminiferal Res.* 25, 53–74, doi:10.2113/gsjfr.25.1.53, 1995.

887 Ravelo, A., Fairbanks, R. and Philander, S.: Reconstructing tropical Atlantic hydrography using planktonic
888 foraminifera and an ocean model, *Paleoceanography*, 5, 409–431, 1990.

889 Regenber, M., Steph, S., Nürnberg, D., Tiedemann, R. and Garbe-Schönberg, D.: Calibrating Mg/Ca
890 ratios of multiple planktonic foraminiferal species with $\delta^{18}\text{O}$ -calcification temperatures: Paleothermometry
891 for the upper water column, *Earth Planet. Sci. Lett.*, 278(3–4), 324–336, doi:10.1016/j.epsl.2008.12.019,
892 2009.

893 Reichart, G.-J., Jorissen, F., Anschutz, P. and Mason, P. R.: Single foraminiferal test chemistry records
894 the marine environment, *Geology*, 31(4), 355–358, 2003.

895 Russell, A. D. and Spero, H. J.: Field examination of the oceanic carbonate ion effect on stable isotopes in
896 planktonic foraminifera, *Paleoceanography*, 15(1), 43–52, 2000.

897 Sadekov, A., Eggins, S. M., De Deckker, P., Ninnemann, U., Kuhnt, W. and Bassinot, F.: Surface and
898 subsurface seawater temperature reconstruction using Mg/Ca microanalysis of planktonic foraminifera
899 *Globigerinoides ruber*, *Globigerinoides sacculifer*, and *Pulleniatina obliquiloculata*, *Paleoceanography*, 24,
900 PA3201, doi:10.1029/2008PA001664, 2009.

901 Schmidt, G.A., G. R. Bigg and E. J. Rohling. 1999. "Global Seawater Oxygen-18 Database - v1.21"
902 <http://data.giss.nasa.gov/o18data/> (last access: 2 November 2014), 1999.

903 Shackleton, N.: Attainment of isotopic equilibrium between ocean water and the benthonic foraminifera
904 genus *Uvigerina*: isotopic changes in the ocean during the last glacial, *Les methods quantitatives d'etude*

905 des variations du climat au cours du Pleistocene, Gif-sur-Yvette, Colloque international du CNRS, 219,
906 203–210, 1974.

907 Spero, H. J. and Lea, D. W.: Intraspecific stable isotope variability in the planktic foraminifera
908 *Globigerinoides sacculifer*: Results from laboratory experiments, Mar. Micropaleontol., 22, 221–234, 1993.

909 Spero, H. J., Lerche, I. and Williams, D. F.: Opening the carbon isotope “vital effect” black box, 2,
910 Quantitative model for interpreting foraminiferal carbon isotope data, Paleoceanography, 6, 639–655,
911 1991.

912 Spero, H. J., Bijma, J., Lea, D. W. and Bemis, B. E.: Effect of seawater carbonate concentration on
913 foraminiferal carbon and oxygen isotopes, Nature, 390, 497–500, doi: 10.1038/37333, 1997.

914 Spero, H. J., Mielke, K. M., Kalve, E. M., Lea, D. W. and Pak, D. K.: Multispecies approach to
915 reconstructing eastern equatorial Pacific thermocline hydrography during the past 360 kyr,
916 Paleoceanography, 18, 1022, doi: 10.1029/2002PA000814, 2003.

917 Steinhardt, J., Cléroux, C., Ullgren, J., de Nooijer, L., Durgadoo, J. V., Brummer, G.-J. and Reichart, G.-J.:
918 Anti-cyclonic eddy imprint on calcite geochemistry of several planktonic foraminiferal species in the
919 Mozambique Channel, Mar. Micropaleontol., 113, 20–33, doi: 10.1016/j.marmicro.2014.09.001, 2014.

920 Steinke, S., Chiu, H., Yu, P., Shen, C., Löwemark, L., Mii, H. and Chen, M.: Mg/Ca ratios of two
921 *Globigerinoides ruber* (white) morphotypes: Implications for reconstructing past tropical/subtropical
922 surface water conditions, Geochem. Geophys. Geosystems, 6, Q11005, 2005.

923 Steph, S., Regenberg, M., Tiedemann, R., Mulitza, S. and Nürnberg, D.: Stable isotopes of planktonic
924 foraminifera from tropical Atlantic/Caribbean core-tops: Implications for reconstructing upper ocean
925 stratification, Mar. Micropaleontol., 71, 1–19, doi: 10.1016/j.marmicro.2008.12.004, 2009.

926 Swallow, J., Fieux, M. and Schott, F.: The boundary currents east and north of Madagascar: 1.
927 Geostrophic currents and transports, J. Geophys. Res. Oceans, 93, 4951–4962, 1988.

928 Tedesco, K., Thunell, R., Astor, Y. and Muller-Karger, F.: The oxygen isotope composition of planktonic
929 foraminifera from the Cariaco Basin, Venezuela: Seasonal and interannual variations, Mar.
930 Micropaleontol., 62, 180–193, doi:10.1016/j.marmicro.2006.08.002, 2007.

931 Tolderlund, D. S. and Bé, A. W.: Seasonal distribution of planktonic foraminifera in the western North
932 Atlantic, Micropaleontology, 17, 297–329, 1971.

933 Ullgren, J., van Aken, H., Ridderinkhof, H. and de Ruijter, W.: The hydrography of the Mozambique
934 Channel from six years of continuous temperature, salinity, and velocity observations, Deep-Sea Res., 69,
935 36–50, 2012.

936 Urey, H. C.: The thermodynamic properties of isotopic substances, J. Chem. Soc. (1926–1965), 562–581,
937 doi:10.1039/JR9470000562, 1947.

938 Vergnaud Grazzini, C.: Non-equilibrium isotopic compositions of shells of planktonic foraminifera in the
939 Mediterranean Sea, Palaeogeogr. Palaeoclimatol. Palaeoecol., 20, 263–276, 1976.

940 Vincent, E. and Berger, W.: Planktonic foraminifera and their use in paleoceanography, The sea, 7, 1025–
941 1119, 1981.

942 Watkins, J. M., Mix, A. C. and Wilson, J.: Living planktic foraminifera: tracers of circulation and productivity
943 regimes in the central equatorial Pacific, Deep Sea Res. Part II Top. Stud. Oceanogr., 43, 1257–1282,
944 1996.

945 Weibull, W.: A statistical theory of the strength of materials, Ingeniorsvetenskaps Akademiens Handlingar
946 NR. 151, 1939.

947 Wefer, G. and Berger, W. H.: Isotope paleontology: growth and composition of extant calcareous species,
948 Mar. Geol., 100, 207–248, 1991.

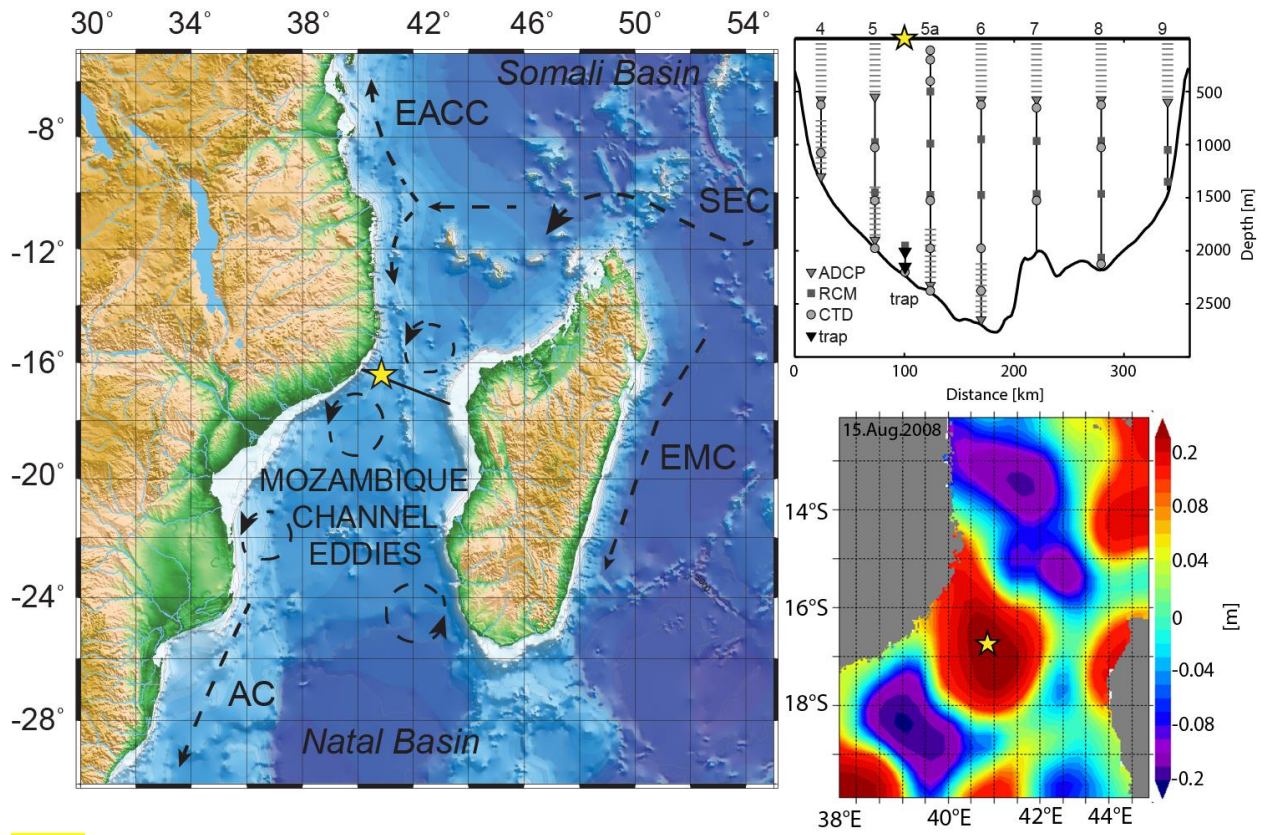
949 Wilke, I., Bickert, T. and Peeters, F. J.: The influence of seawater carbonate ion concentration [CO₃²⁻] on
950 the stable carbon isotope composition of the planktic foraminifera species *Globorotalia inflata*, Mar.
951 Micropaleontol., 58, 243–258, 2006.

952 Wilke, I., Meggers, H. and Bickert, T.: Depth habitats and seasonal distributions of recent planktic
953 foraminifers in the Canary Islands region (29°N) based on oxygen isotopes, Deep Sea Res., 56, 89–106,
954 doi: 10.1016/j.dsr.2008.08.001, 2009.

955 Wyrтки, K.: Physical oceanography of the Indian Ocean, in The biology of the Indian Ocean, Springer,
956 Berlin Heidelberg, 18–36, 1973.

957

958 **Figures:**



959 **Fig. 1**

961

species	Mg/Ca [mmol/mol]	Mg/Ca SD [mmol/mol]	Mg/Ca-based temperatures [°C]	$\delta^{18}\text{O}$ [‰]	$\delta^{18}\text{O}$ SD [‰]	$\delta^{18}\text{O}$ -based temperatures [°C]	$\delta^{13}\text{C}$ ±SE [‰]	$\delta^{13}\text{C}$ SD [‰]
<i>G. ruber</i>	5.3±0.09	±1.2	28.1±2.8	-2.57±0.04	±0.35	29.4±1.3	0.51±0.03	±0.47
<i>N. dutertrei</i>	2.6±0.06	±1.0	22.5±3.7	-1.53±0.03	±0.48	24.3±2.0	0.53±0.04	±0.44
<i>P. obliquiloculata</i>	2.3±0.1	±0.6	21.6±3.1	-1.13±0.04	±0.24	22.3±1.1	0.04±0.04	±0.21
<i>G. scitula</i>	1.5±0.07	±0.4	14.4±3.4	1.47±0.14	±0.87	14.4±3.9*	0.27±0.04	±0.22

* vital effect corrected [Kahn an Williams, 1981]

data from Steinhardt et al. 2014

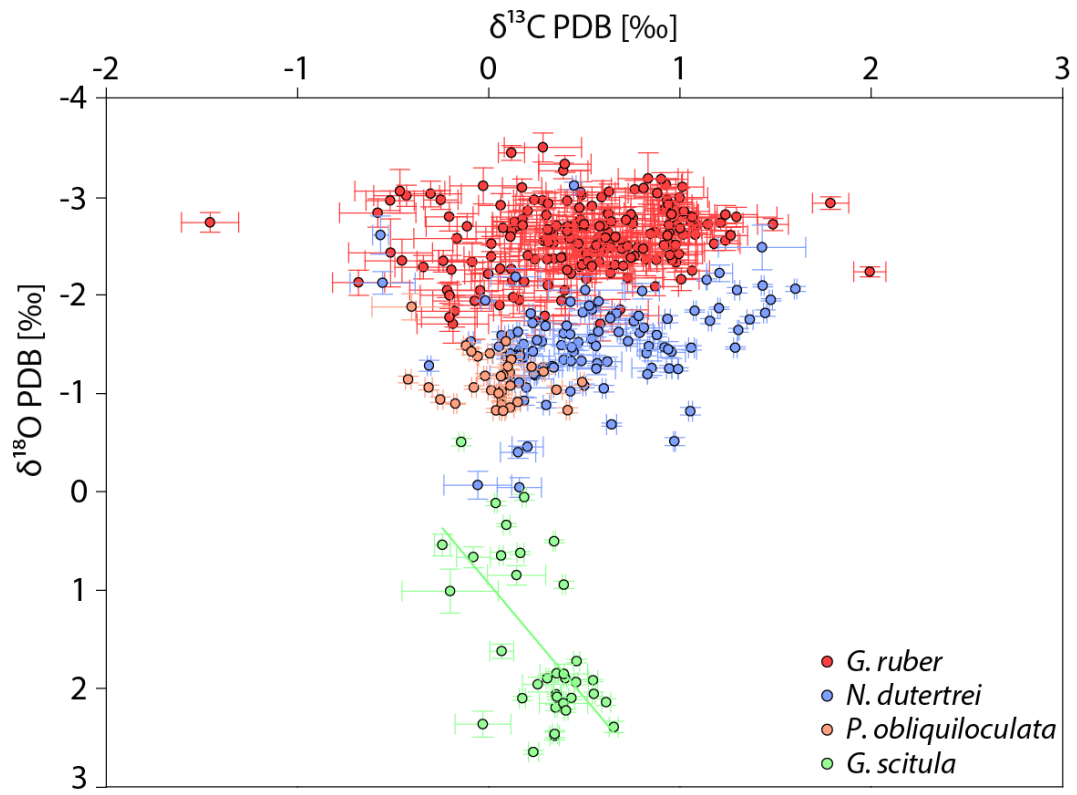
962 **Tab. 1**

963

species	$\delta^{13}\text{C}$ [‰]		$\delta^{13}\text{C}$ SD [‰]		$\delta^{18}\text{O}$ [‰]		$\delta^{18}\text{O}$ SD [‰]	
	VU	BCN	VU	BCN	VU	BCN	VU	BCN
<i>G. rub</i>	-	0.51±0.03	-	±0.47	-	-2.57±0.04	-	0.35
<i>N. dut</i>	0.41±0.12	0.54±0.01	0.41	0.45	-1.37±0.09	-1.58±0.03	0.59	0.46
<i>P. obli</i>	-0.07±0.13	0.05±0.01	0.29	0.20	-1.46±0.09	-1.10±0.02	0.37	0.21
<i>G. scit</i>	0.13±0.14	0.3±0.02	0.24	0.21	1.55±0.11	1.45±0.04	0.69	0.92

964 **Tab. 2**

965



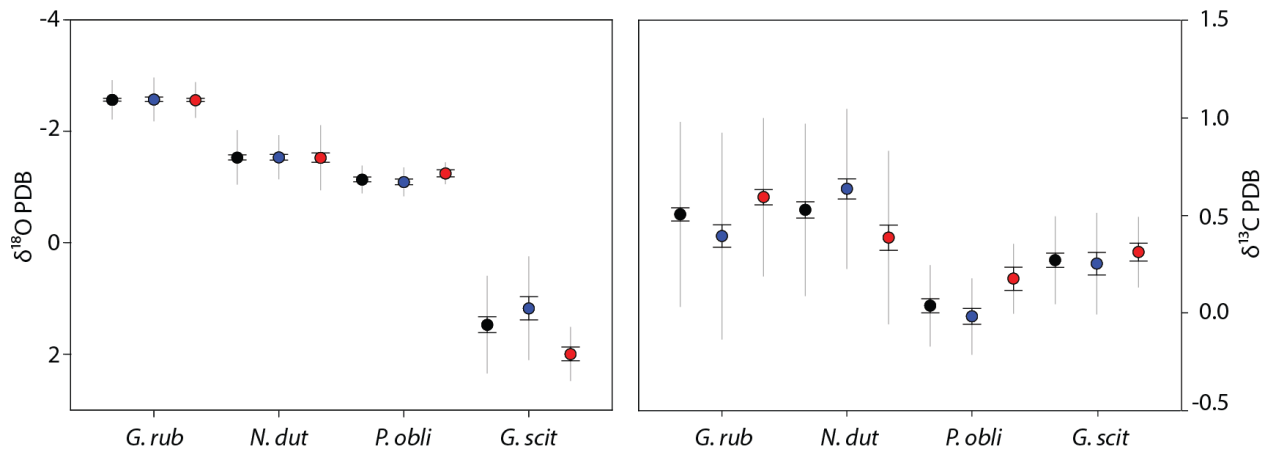
966

967 **Fig. 2**

Species	$\delta^{18}\text{O} \pm \text{SE}$ [‰]		$\delta^{18}\text{O}$ SD [‰]		T [°C], (Kim&O'Neil, 1997)		$\delta^{13}\text{C} \pm \text{SE}$ [‰]		$\delta^{13}\text{C}$ SD [‰]	
	Eddy	Non-Eddy	Eddy	Non-Eddy	Eddy	Non-Eddy	Eddy	Non-Eddy	Eddy	Non-Eddy
<i>G. ruber</i>	-2.56±0.03	-2.57±0.04	0.31	0.39	29.8	29.2	0.59±0.04	0.39±0.06	0.40	0.53
<i>N. dutertrei</i>	-1.53±0.08	-1.53±0.05	0.58	0.39	24.6	24.0	0.39±0.06	0.64±0.04	0.44	0.41
<i>P. obliquiloculata</i>	-1.25±0.06	-1.09±0.05	0.19	0.25	23.3	21.9	0.18±0.06	-0.02±0.04	0.18	0.19
<i>G. scitula</i>	1.99±0.1	1.18±0.2	0.48	0.92	8.2	11.5	0.31±0.05	0.25±0.06	0.18	0.26

968 **Tab. 3**

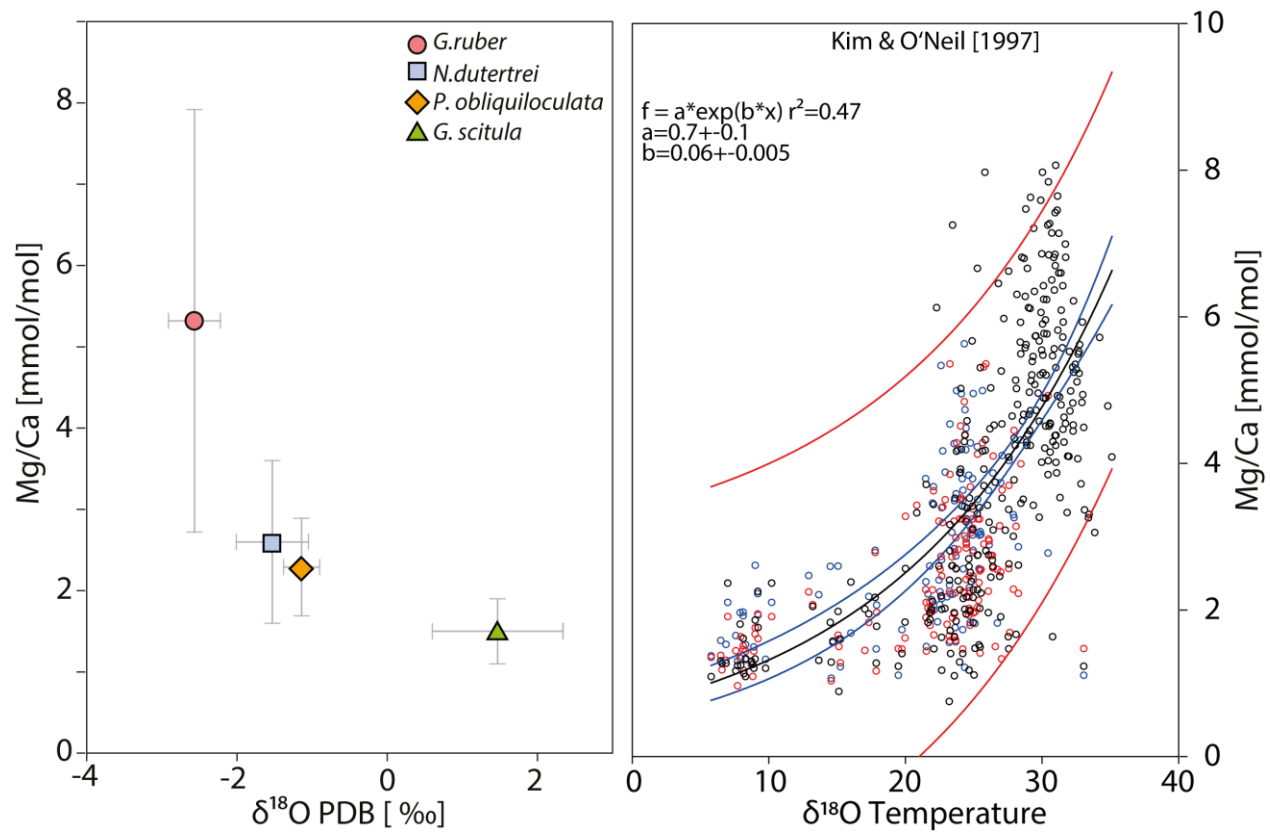
969



970

971

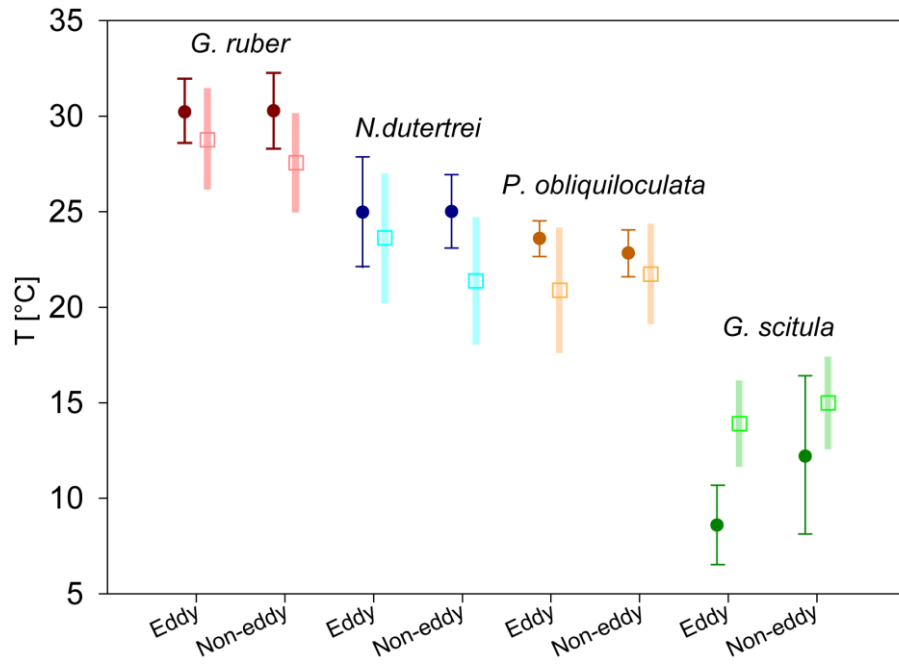
972 **Figure 3**



973

974 **Figure 4**

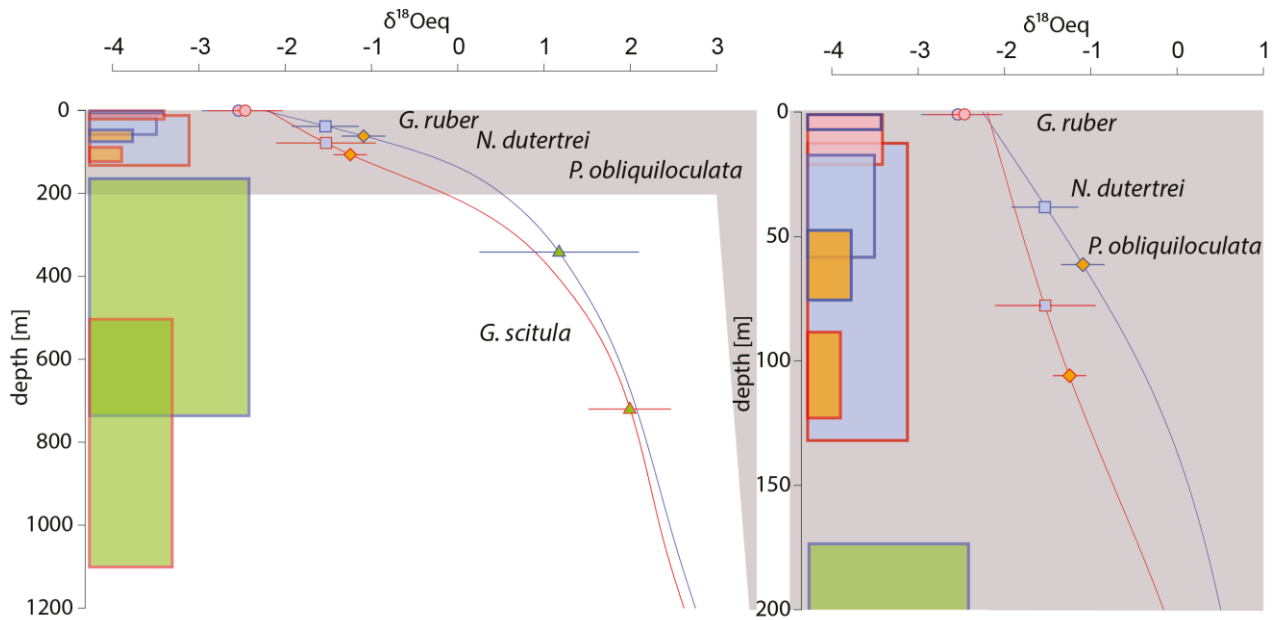
975



976

977 **Figure 5**

978

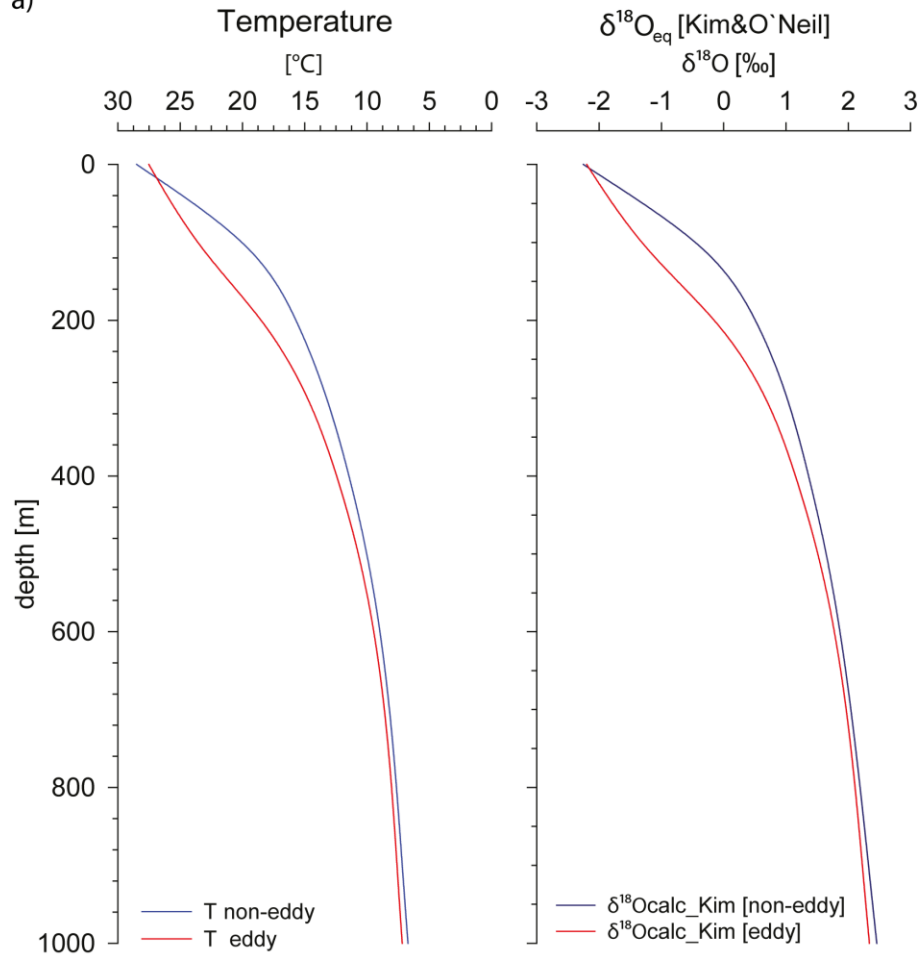


979

980 **Figure 6**

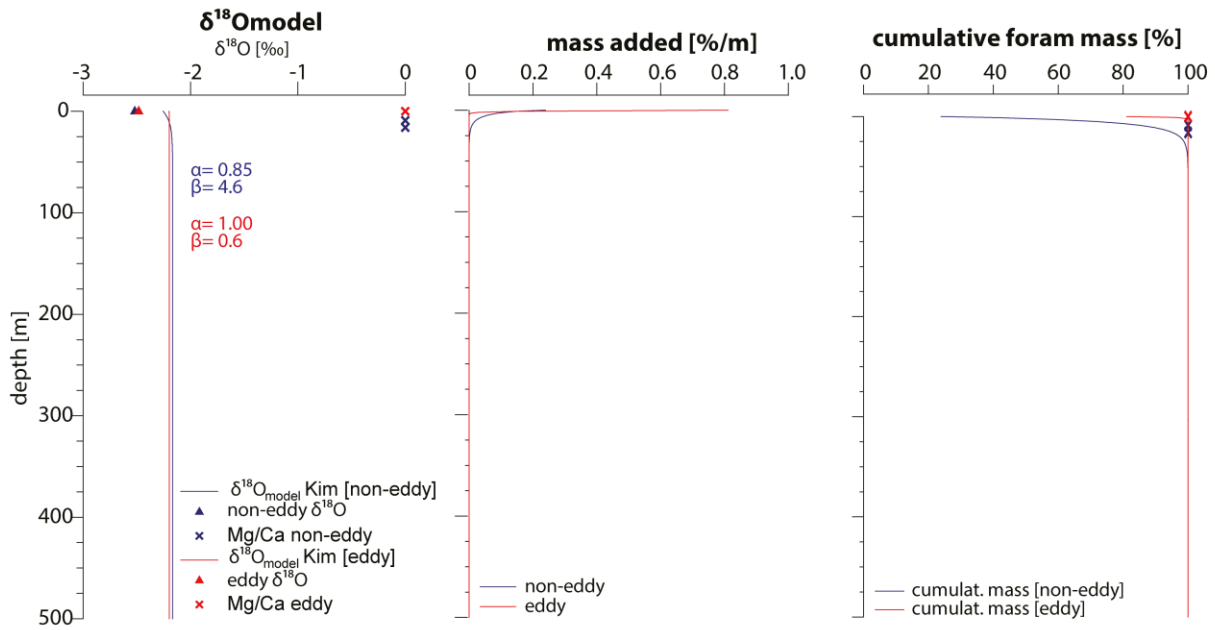
981

a)



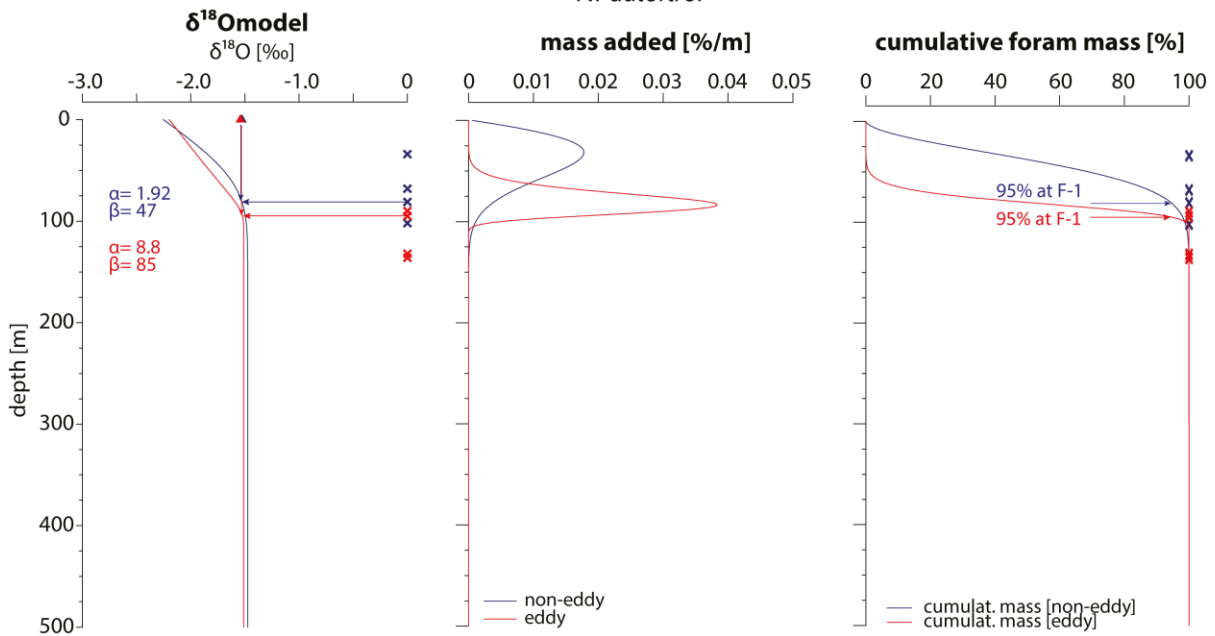
b)

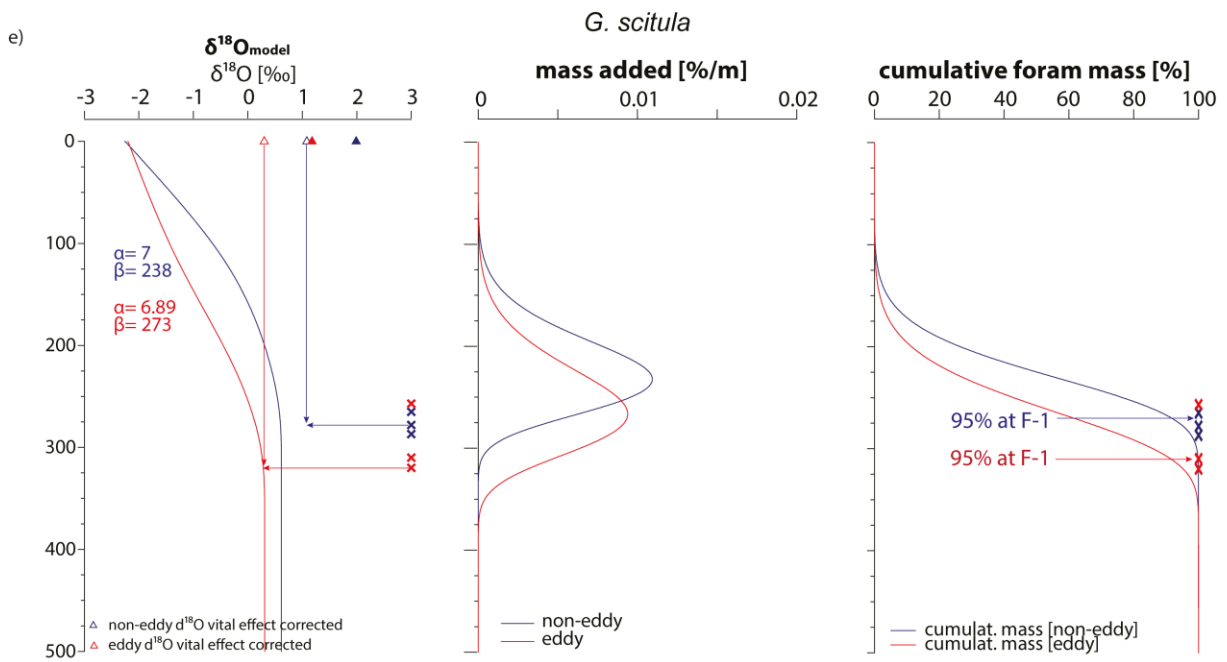
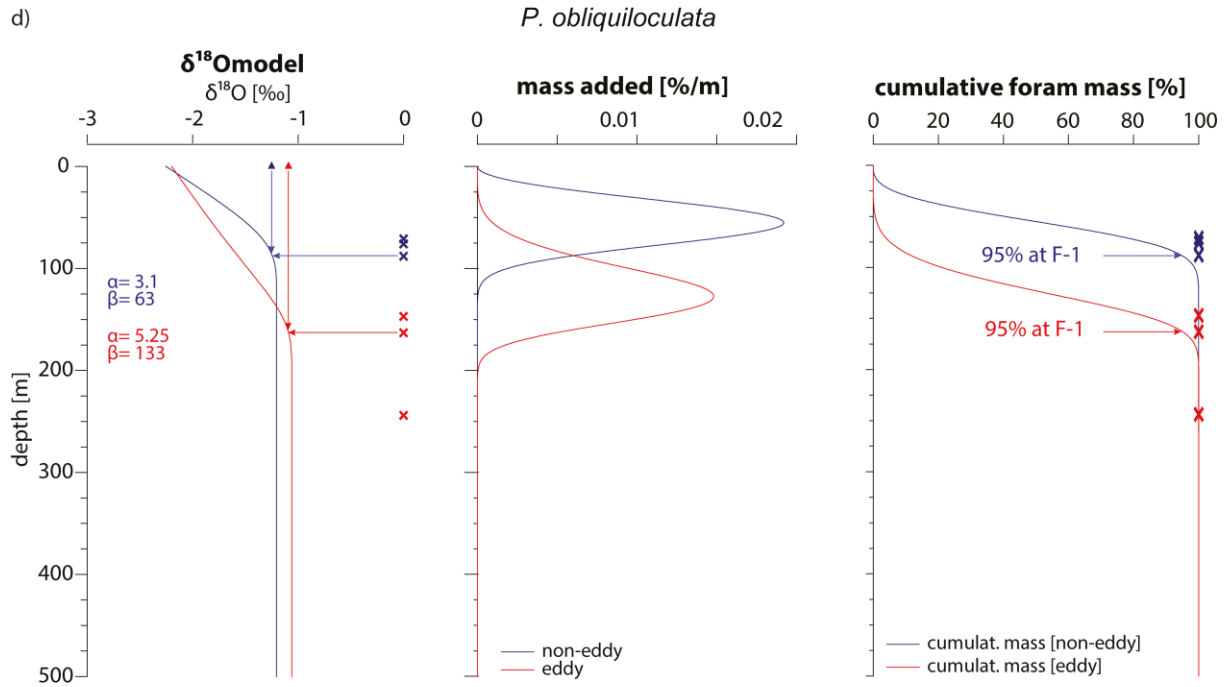
G. ruber



c)

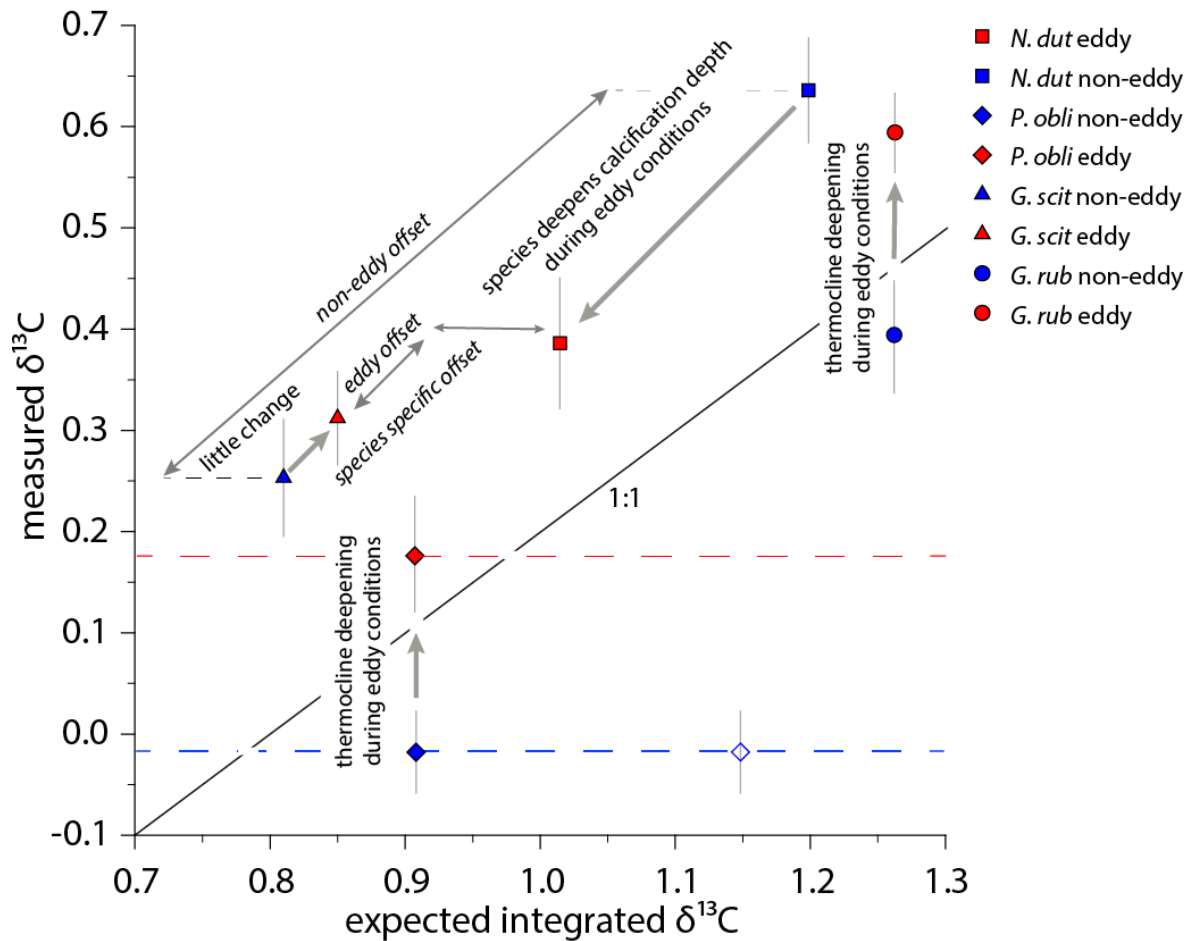
N. dutertrei





984
 985 **Figure 7**

986



987

988 *Figure 8*

989

990 **Figure captions:**

991

992 *Figure 1:* Hydrography of southwestern Indian Ocean and location of the sediment trap (star)
 993 within the mooring array (right top). On the right bottom a map of sea level anomaly shows the
 994 passing of an anti-cyclonic eddy over the trap location (star). AVISO sea level anomaly map was
 995 produced using the AVISO live access server (<http://las.aviso.altimetry.fr/las/getUI.do>). EACC:
 996 East African Coastal Current, SEC: South Equatorial Current, AC: Agulhas Current.

997

998 *Table 1:* Average Mg/Ca ratios (Steinhardt et al., 2014), $\delta^{18}\text{O}$ and $\delta^{13}\text{C}$ with standard errors (SE)
 999 and corresponding standard deviations (SD). Mg/Ca-based temperature are based on species
 1000 specific temperature equations. The equation developed by Fallet et al. (2010) was applied for
 1001 *G. ruber*. The equations developed by Anand et al. (2003) were applied to *N. dutertrei*, *P.*
 1002 *obliciloculata*. For *G. scitula* Anand's equation for *G. hirsuta* was applied following the example
 1003 of Fallet et al. (2011). Calculate $\delta^{18}\text{O}$ -based temperatures are based on the equation of Kim and
 1004 O'Neil (1997).

1005

1006 *Table 2: Average measurements of $\delta^{18}\text{O}$ and $\delta^{13}\text{C}$ with standard errors (SE) and corresponding*
1007 *standard deviations (SD) performed at the Universitat Autònoma de Barcelona on a Thermo*
1008 *Finnigan MAT253 mass spectrometer coupled to a Kiel IV device for CO₂ sample gas*
1009 *preparation (BCN) and the Thermo Finnigan Delta Plus mass spectrometer equipped with a Gas*
1010 *Bench II preparation device at the VU University Amsterdam (VU). Measurements of *N.**
1011 **dutertrei*, *P. obliquiloculata* and *G. scitula* are comparable and species-specific values are in*
1012 *good agreement*

1013
1014 *Figure 2: Scatter plot of single shell $\delta^{13}\text{C}$ versus $\delta^{18}\text{O}$ with analytical error. Note the linear*
1015 *relation in *G. scitula* ($r^2=0.388$, $p<0.001$).*

1016 *Figure 3: Eddy (red circles), non-eddy (blue circles) comparison of $\delta^{13}\text{C}$ PDB and $\delta^{18}\text{O}$ PDB for*
1017 *the analyzed species. Grey lines indicate standard deviation (SD), black capped lines are*
1018 *indicative of standard error (SE).*

1019 *Table 3: Results for $\delta^{18}\text{O}$ and $\delta^{13}\text{C}$ with standard errors (SE) and corresponding standard*
1020 *deviations (SD) under eddy and non-eddy conditions for *G. ruber*, *N. dutertrei*, *P. obliquiloculata**
1021 *and *G. scitula*.*

1022
1023 *Figure 4: Scatter plot of Mg/Ca versus $\delta^{18}\text{O}_{\text{cc}}$ (left panel). Right panel: single chamber Mg/Ca*
1024 *exponential relationship with $\delta^{18}\text{O}$ -derived Temperatures calculated using Kim & O'Neil (1997).*
1025 *Regression: $f = a \cdot \exp(b \cdot x)$, with $a=-0.7$, $b=0.06$, $r^2=0.47$ using F-1/2 Mg/Ca from *G. ruber*, F-0*
1026 *for *N. dutertrei*, *P. obliquiloculata* and *G. scitula* (black circles). F-1 for *N. dutertrei*, *P.**
1027 **obliquiloculata* and *G. scitula* (red circles) and F-2 for *N. dutertrei*, *P. obliquiloculata* and *G.**
1028 **scitula* (blue circles). Mg/Ca data from Steinhardt et al. (2014). Note that the correlation*
1029 *coefficient also indicates that approximately 60% of the observed variability is not due to*
1030 *temperature alone.*

1031 *Figure 5: Inter-species $\delta^{18}\text{O}$ - and Mg/Ca-derived temperature for eddy and non-eddy intervals.*
1032 *Circles: $\delta^{18}\text{O}$ -based temperatures using the equation of Kim and O'Neil (1997), Squares*
1033 *represent Mg/Ca-based temperatures using the species specific equations of Anand et al.*
1034 *(2003) for *N. dutertrei*, *P. obliquiloculata* and *G. scitula*. For *G. ruber*, the equation of Fallet et al.*
1035 *(2011) was used. Vertical error bars (SD) for $\delta^{18}\text{O}$ derived temperatures, horizontal error bars*
1036 *(SD) for Mg/Ca derived temperatures. Red colors: *G. ruber*, blue: *N. dutertrei*, orange: *P.**
1037 **obliquiloculata*, green: *G. scitula*.*

1038
1039 *Figure 6: Apparent calcification depths of species are generally shallower during non-eddy*
1040 *conditions. Apparent calcification depths for eddy (red) and non-eddy conditions (blue)*
1041 *calculated from single specimen $\delta^{18}\text{O}_{\text{cc}}$ using *in situ* temperature and $\delta^{18}\text{O}_{\text{w}}$. Calcification depth*
1042 *was determined by matching the measured foraminiferal $\delta^{18}\text{O}_{\text{cc}}$ with the $\delta^{18}\text{O}_{\text{eq}}$, using the*
1043 *equation of Kim and O'Neil (1997). We used $\delta^{18}\text{O}_{\text{sw}}$ from the species calcification depth. Grey*
1044 *box indicates the zone of the close-up on the right (upper 200 m).*

1045 *Figure 7: Cumulative calcification model for eddy (red) and non-eddy (blue) conditions from left*
1046 *to right: temperature profiles as well as $\delta^{18}\text{O}_{\text{equilibrium}}$ ($\delta^{18}\text{O}_{\text{eq}}$) for the upper 1000 m and*

1047 $\delta^{18}\text{O}_{\text{cumulative}}$ ($\delta^{18}\text{O}_{\text{model}}$) for the upper 500m (a). On the upper far right, mass
1048 development/growth pattern, below cumulative mass of the foraminifera (foram mass) is plotted
1049 for the upper 500 m. Bulk $\delta^{18}\text{O}_{\text{foram}}$ (triangles) Mg/Ca derived single chamber calcification depth
1050 (crosses) are indicated in the relevant plots for *G. ruber* (b), *N. dutertrei* (c), *P. obliquiloculata* (c)
1051 and *G. scitula* (d)

1052 *Figure 8*: Inter-species differences between expected $\delta^{13}\text{C}$ values, based on the cumulative
1053 mass balance model, and measured $\delta^{13}\text{C}$ values of *G. ruber*, *N. dutertrei*, *P. obliquiloculata* and
1054 *G. scitula*. Dashed line indicates the 1:1 line of measured and expected $\delta^{13}\text{C}$. Red symbols
1055 represent values for eddy conditions, blue symbols represent values for non-eddy condition.
1056 Thick grey arrows indicate intra-species trends between non-eddy and eddy conditions, thin
1057 arrows indicate inter-specific trends. *P. obliquiloculata* does not calcify in isotopic equilibrium
1058 with dissolved ΣCO_2 , but the deviation from isotopic equilibrium is a linear function of
1059 temperature (Mulitza et al., 1999), hence there is no projected $\delta^{13}\text{C}_{\text{expect}}$, this is indicated by the
1060 dotted lines. Open diamond indicates $\delta^{13}\text{C}_{\text{expect}}$ for *P. obliquiloculata* non-eddy conditions.

1061